Journal of Systematic Palaeontology

ISSN: (Print) (Online) Journal homepage: https://www.tandfonline.com/loi/tjsp20

A new longirostrine sperm whale (Cetacea, Physeteroidea) from the lower Miocene of the Pisco Basin (southern coast of Peru)

Olivier Lambert , Christian de Muizon , Mario Urbina & Giovanni Bianucci

To cite this article: Olivier Lambert , Christian de Muizon , Mario Urbina & Giovanni Bianucci (2020) A new longirostrine sperm whale (Cetacea, Physeteroidea) from the lower Miocene of the Pisco Basin (southern coast of Peru), Journal of Systematic Palaeontology, 18:20, 1707-1742, DOI: 10.1080/14772019.2020.1805520

To link to this article: https://doi.org/10.1080/14772019.2020.1805520

Journal of Systematic Palaeontology, 2020
Vol. 18, No. 20, 1707–1742, http://dx.doi.org/10.1080/14772019.2020.1805520

A new longirostrine sperm whale (Cetacea, Physeteroidea) from the lower Miocene of the Pisco Basin (southern coast of Peru)

Olivier Lambert[a]*, Christian de Muizon[b], Mario Urbina[c] and Giovanni Bianucci[d]

[a]*Direction Opérationnelle Terre et Histoire de la Vie, Institut royal des Sciences naturelles de Belgique, Brussels, Belgium;* [b]*CR2P UMR 7207, (MNHN, CNRS, UPMC, Sorbonne-Université), Muséum national d'Histoire naturelle, Département Origines et Evolution, Paris, France;* [c]*Departamento de Paleontología de Vertebrados, Museo de Historia Natural – UNMSM, Lima, Peru;* [d]*Dipartimento di Scienze della Terra, Università di Pisa, Pisa, Italy*

(Received 11 February 2020; accepted 28 July 2020)

The modern sperm whales *Kogia* and *Physeter* (superfamily Physeteroidea) represent highly disparate, relict members of a group of odontocetes that peaked in diversity during the middle to late Miocene. Based on a highly informative specimen (including the cranium with ear bones, mandibles, teeth and some postcranial elements) from the lower Miocene (early Burdigalian, 19–18 Ma) of the Chilcatay Formation (Pisco Basin, Peru), we describe here a new genus and species of physeteroid, *Rhaphicetus valenciae* gen. et sp. nov. The latter is one of the geologically oldest physeteroids. This medium-sized species (estimated body length between 4.7 and 5.7 m) differs from all other physeteroids by the following, probably autapomorphic, features: a narrow, cylindrical rostrum comprising nearly 75% of the condylobasal length; the two main dorsal infraorbital foramina located posterior to the antorbital notch; an upper tooth count of at least 36 teeth per quadrant; and anterior-most upper alveoli filled by thick bony pads. Our phylogenetic analysis recovers *R. valenciae* as one of the earliest branching stem physeteroids. The highly unusual filling of the anterior upper alveoli by bony pads is interpreted as part of a mechanism leading to the loss of apical and subapical upper teeth. By comparison with other odontocetes displaying some degree of anterior reduction of the dentition, this condition may have corresponded to the rostrum being anteriorly longer than the mandible. The elongated rostrum with a circular cross-section, the long temporal fossa, and the high number of slender, pointed upper and lower teeth all suggest that *R. valenciae* used its dentition to grasp relatively small prey, possibly via rapid movements of the head. On the one hand, this new Peruvian record increases our knowledge of the morphological disparity of sperm whales during the Miocene. On the other hand, it may provide clues to the ancestral morphotype for all physeteroids.

http://zoobank.org/urn:lsid:zoobank.org:pub:3E1CEFC8-0F23-416E-9C02-03750D7199BA

Keywords: Burdigalian; dental reduction; functional morphology; palaeobiology; phylogeny; stem Physeteroidea

Introduction

Although representing only a remnant of their past diversity, which peaked during the middle to late Miocene (Velez-Juarbe *et al.* 2015; Lambert *et al.* 2017; Paolucci *et al.* 2020), the morphological disparity of extant sperm whales (Cetacea, Physeteroidea) is remarkable. On the one hand, the great sperm whale, *Physeter macrocephalus*, is the largest modern odontocete, with adult male body length reaching 18 m, and a rostrum that is proportionally long and broad, excavated by the anterior extension of a vast supracranial basin, containing the large spermaceti organ and junk (Rice 1989; Cranford 1999; Huggenberger *et al.* 2016). On the other hand, the dwarf and pygmy sperm whales, *Kogia sima* and *Kogia breviceps*, average 2.7 and 3.4 m in standard body length, respectively, and, among other unusual morphological features (for example in the soft tissue forehead), display an extremely abbreviated rostrum (the shortest among extant odontocetes) and surprisingly slender and pointed lower teeth (Caldwell & Caldwell 1989; Werth 2006; Thornton *et al.* 2015). Despite this marked morphological disparity, *Kogia* and *Physeter* are both interpreted as highly specialized mesopelagic suction feeders, predominantly preying upon cephalopods, and sharing several morphological features related to this feeding strategy, for example a strongly reduced upper dentition (vestigial or completely absent), a slender lower jaw, and a small temporal fossa for the main jaw adductor muscles (Flower 1867a; Schulte & Smith 1918; Boschma 1938; Caldwell & Caldwell 1989; Werth 2004, 2006; Bloodworth & Marshall 2005; Watwood *et al.* 2006; Staudinger *et al.* 2014).

*Corresponding author. Email: olivier.lambert@naturalsciences.be

Published online 21 Sep 2020

When expanding this assessment of morphological disparity to the fossil record of physeteroids, possibly traced back to the latest Oligocene (Marx *et al.* 2016), the range of skull morphologies is further increased, for example with the aberrant kogiids in the subfamily Scaphokogiinae, displaying a unique morphology of the supracranial basin and rostrum (Muizon 1984; Benites-Palomino *et al.* 2020; Collareta *et al.* in press), and the medium- to giant-sized macroraptorial stem physeteroids, bearing proportionally much larger teeth on robust upper and lower jaws (Bianucci & Landini 2006; Kimura *et al.* 2006; Boersma & Pyenson 2015; Lambert *et al.* 2017).

In this work we describe and compare a new medium-sized stem physeteroid from the lower Miocene of the Chilcatay Formation (Pisco Basin, southern coast of Peru), a unit that recently yielded a large number of odontocete taxa (e.g. Lambert *et al.* 2015, 2018; Bianucci *et al.* 2018a, b; Di Celma *et al.* 2018, 2019). We investigate the phylogenetic relationships of the new taxon and discuss the ecological implications of the novel rostrum morphology observed in one of the geologically oldest sperm whales.

Material and methods

Institutional abbreviations

IRSNB, Institut royal des Sciences naturelles de Belgique, Brussels, Belgium; **LACM,** Natural History Museum of Los Angeles County, Los Angeles, USA; **MAUS,** Museo dell'Ambiente dell'Università del Salento, Lecce, Italy; **MLP,** Museo de La Plata, La Plata, Argentina; **MNHN,** Muséum national d'Histoire naturelle, Paris, France; **MSNUP,** Museo di Storia Naturale, Università di Pisa, Pisa, Italy; **MUSM,** Museo de Historia Natural, Universidad Nacional Mayor de San Marco, Lima, Peru; **NNML,** Naturalis, Leiden, The Netherlands; **OU,** University of Otago, Dunedin, New Zealand; **USNM,** National Museum of Natural History, Smithsonian Institution, Washington, DC, USA; **ZMA,** Zoölogisch Museum Amsterdam, The Netherlands (now housed at NNML).

Studied material

The main specimen of this work, the partial skeleton MUSM 2543, was discovered by M. Urbina, collected by him and W. Aguirre, and mechanically prepared by the latter at MUSM. Preparation was finalized by O. Lambert for the cranium and detached ear bones. Comparative material (mostly extant and extinct physeteroids) was consulted in the following institutions: IRSNB, LACM, MAUS, MNHN, MSNUP, MUSM, NNML, OU, USNM and ZMA.

Anatomical terminology

For the anatomical terminology of the skull we primarily follow Mead & Fordyce (2009). For a few morphological features more specific to physeteroids we follow Flower (1867a), Kellogg (1927, 1965) and Bianucci & Landini (2006).

Phylogenetic analysis

We coded the specimen MUSM 2543 in the character-taxon matrix of Collareta *et al.* (in press), modified from Lambert *et al.* (2017) and Collareta *et al.* (2019) (see list of characters and character-taxon matrix in Supplementary material 1, 2). We provisionally removed the small physeteroid *Thalassocetus antwerpiensis* from the matrix, as this taxon is currently being reassessed (Alfsen *et al.* in press). Differing from other recent analyses (Benites-Palomino *et al.* 2020; Paolucci *et al.* 2020), due to the fragmentary state of the type material (Boersma & Pyenson, 2015) and considering the relatively limited number of characters in our matrix, we chose not to include the macroraptorial species *Albicetus oxymycterus* in our cladistic analysis. The analysis was undertaken with PAUP* (Swofford 2001), with the same settings as in Collareta *et al.* (in press), i.e. heuristic search with all characters unordered and all default settings of the software (including tree bisection and reconnection with reconnection limit = 8 and ACCTRAN optimization). Three outgroups were defined *a priori*, the basilosaurids *Cynthiacetus* and *Zygorhiza* and the archaic odontocete *Agorophius*. Node support was evaluated through calculation of bootstrap values (100 replicates).

Systematic palaeontology

Order **Cetacea** Brisson, 1762
Pelagiceti Uhen, 2008
Neoceti Fordyce & Muizon, 2001
Suborder **Odontoceti** Flower, 1867b
Superfamily **Physeteroidea** Gray, 1821
Genus ***Rhaphicetus*** gen. nov.

Type species. *Rhaphicetus valenciae* sp. nov.

Derivation of name. From the ancient Greek *rhaphis*, needle, and from the Latin *cetus*, whale: the whale with a needle-shaped rostrum.

Diagnosis. As for the only included species.

Rhaphicetus valenciae sp. nov.

Holotype. MUSM 2543, a partial, disarticulated skeleton including the sub-complete cranium with ear bones (periotics, tympanic bulla, malleus, incus and stapes), partial mandibles, detached teeth, thoracic, lumbar and caudal vertebrae, a sternum fragment and partial ribs.

Type locality. Zamaca, East Pisco Basin, on the western side of the Ica River, about 60 km SSE of the city of Ica, southern coast of Peru (Fig. 1A, B). MUSM 2543 was listed as specimen ZM 27 in the map of the Zamaca fossil locality by Di Celma *et al.* (2019). Geographical coordinates: 14°36'44.3"N, 75°38'59.3"W.

Type horizon and age. Chilcatay Formation, 34.7 m above the base of the local geological section, in allomember Ct1, facies association Ct1a (see Di Celma *et al.* 2019) (Fig. 1D). ^{39}Ar–^{40}Ar dating of local ash layers constrains the age of the level where MUSM 2543 was found to an interval ranging from 19.0 to 18.02 Ma, early Burdigalian (late early Miocene; Di Celma *et al.* 2018; Bosio *et al.* 2020a). Based on ^{87}Sr/^{86}Sr ages obtained from samples taken in Ullujaya and Zamaca (see Bosio *et al.* 2020b) the age could be further restricted to 18.6–18.0 Ma. The odontocete-rich associated vertebrate fauna in Ct1a includes eurhinodelphinids, the homodont, longirostrine odontocete *Chilcacetus cavirhinus*, kentriodontids, other physeteroids and several platanistoids (including the squalodelphinids *Huaridelphis raimondii* and *Notocetus vanbenedeni*), together with sea turtles, and osteichthyan and elasmobranch fishes (Di Celma *et al.* 2018, 2019; Landini *et al.* 2019).

Derivation of name. *valenciae*, honouring Dr Niels Valencia Marciano Chacón, a biologist at the Universidad Nacional Mayor de San Marcos studying plant ecology and the director of the MUSM, for his constant support for the palaeontological activities at that institution, including many fruitful palaeontological expeditions in the Pisco Basin.

Diagnosis. *Rhaphicetus valenciae* is unambiguously identified as a physeteroid due to (1) the presence of a large supracranial basin in the facial region of the cranium; (2) the marked asymmetry of the bony nares (left naris much larger than the right); (3) an enlarged accessory ossicle occupying a vast area of the ventral surface of the anterior process of the periotic (shared with *Inticetus*), and (4) a strong concavity at midlength of the dorsomedial surface of the involucrum of the tympanic bulla.

This medium-sized member of the superfamily is characterized by several possibly autapomorphic features: narrow, cylindrical rostrum comprising nearly 75% of the condylobasal length; the two main dorsal infraorbital foramina located significantly more posterior than the antorbital notch on both the right and left maxillae; upper tooth count of at least 36 teeth per row; and anterior-most upper alveoli filled by thick bony pads.

Rhaphicetus valenciae can be further distinguished from all other physeteroids by the following unique combination of characters: small supracranial basin, proportionally narrow (55% of bizygomatic width) and not extending significantly along the dorsal surface of the rostrum; antorbital notch 'U'-shaped and located outside the supracranial basin; right premaxillary foramen posterior to the level of the antorbital notch; retention of a medium-sized left premaxillary foramen; right premaxilla not covering the whole lateral wall of the supracranial basin; posterior end of each maxilla beyond the supracranial basin being remote from the sagittal plane; frontal-maxilla suture making an angle of 10–15° to the horizontal above the orbit in lateral view; temporal fossa anteroposteriorly longer than dorsoventrally high; styliform process of the jugal displaying a long contact with the zygomatic process of the squamosal; zygomatic process of the squamosal elongated (ratio between distance from anterior tip of zygomatic process to ventral tip of postglenoid process and bizygomatic width greater than 0.33); dorsal edge of zygomatic process remaining roughly rectilinear posteriorly until a level beyond the postglenoid process; postglenoid process of the squamosal ventrally longer than the posttympanic process, the latter being also anteroposteriorly short; joined hamular processes of the pterygoids posteromedially pointed; articular surfaces of the occipital condyles facing posterodorsally; dorsal process of the periotic moderately developed; presence of a marked facet for the sigmoid process of the tympanic on the lateral tuberosity of the periotic; posterior process of the periotic not plate-like; retention of a short tubercule on the malleus; ventral margin of the mandible nearly rectilinear; proportionally small teeth (ratio between maximum root diameter and bizygomatic width of the skull lower than 0.03); short crown of teeth covered by a thin (< 0.25 mm) layer of enamel; enamel on teeth smooth, lacking any ornamentation; and centra of the lumbar vertebrae longer than wide or high.

Description of *Rhaphicetus valenciae* MUSM 2543

Ontogenetic stage. All of the thoracic, lumbar and caudal vertebrae of MUSM 2543 that preserve the anterior and/or posterior region of the centrum display closed

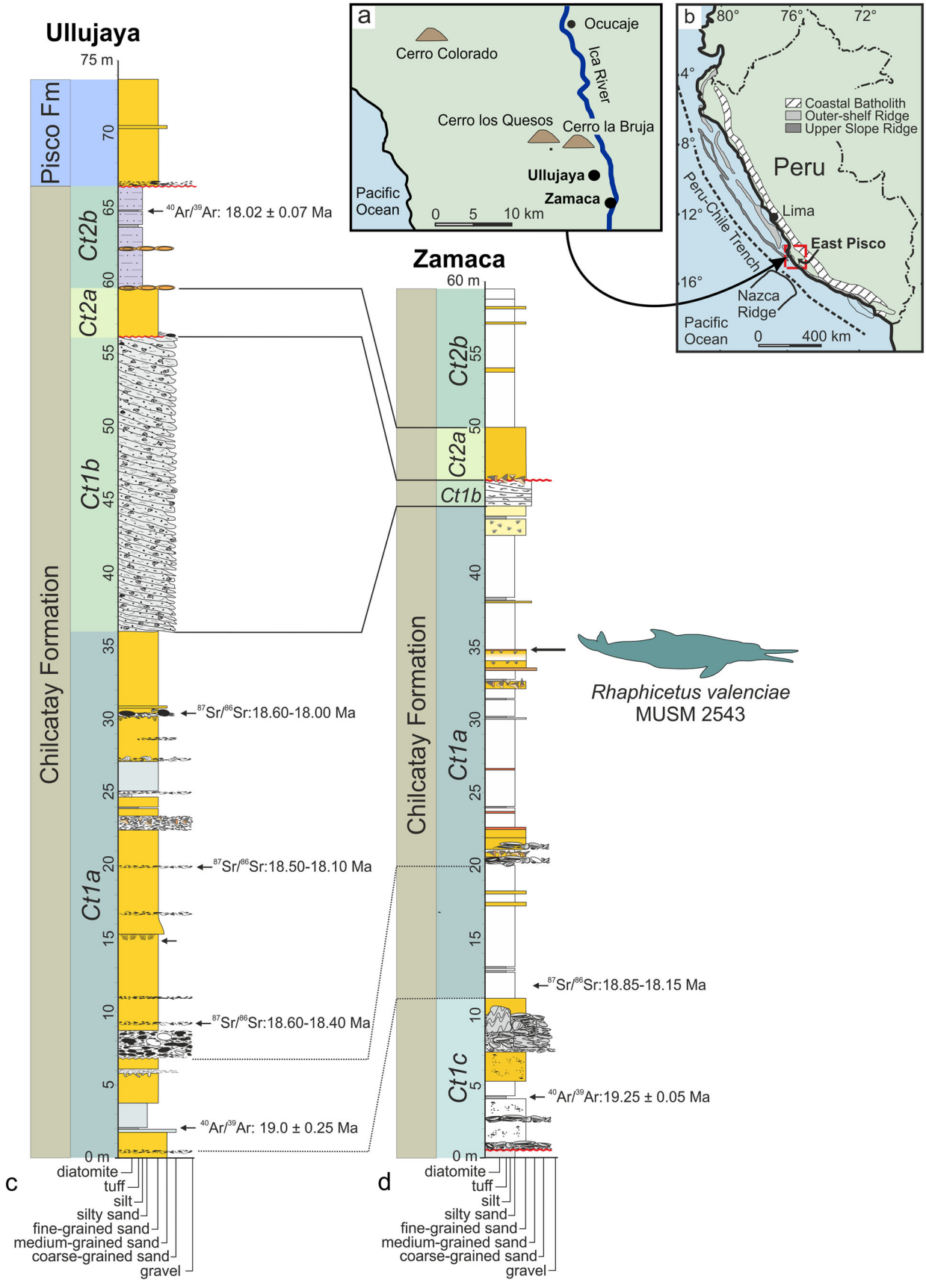
Ullujaya
75 m
Pisco Fm
Chilcatay Formation
Ct2b
Ct2a
Ct1b
Ct1a
^{40}Ar/^{39}Ar: 18.02 ± 0.07 Ma
^{87}Sr/^{86}Sr:18.60-18.00 Ma
^{87}Sr/^{86}Sr:18.50-18.10 Ma
^{87}Sr/^{86}Sr:18.60-18.40 Ma
^{40}Ar/^{39}Ar: 19.0 ± 0.25 Ma
0 m
c
diatomite
tuff
silt
silty sand
fine-grained sand
medium-grained sand
coarse-grained sand
gravel
a
Ocucaje
Cerro Colorado
Ica River
Cerro los Quesos
Cerro la Bruja
Ullujaya
Zamaca
Pacific Ocean
0 5 10 km
b
80°
76°
72°
4°
8°
12°
16°
Coastal Batholith
Outer-shelf Ridge
Upper Slope Ridge
Peru
Peru-Chile Trench
Lima
East Pisco
Nazca Ridge
Pacific Ocean
0 400 km
Zamaca
60 m
Ct2b
Ct2a
Ct1b
Ct1a
Ct1c
Chilcatay Formation
Rhaphicetus valenciae
MUSM 2543
^{87}Sr/^{86}Sr:18.85-18.15 Ma
^{40}Ar/^{39}Ar:19.25 ± 0.05 Ma
0 m
d
diatomite
tuff
silt
silty sand
fine-grained sand
medium-grained sand
coarse-grained sand
gravel

but not fully fused sutures for epiphyses, a strong clue for the interpretation of this specimen as fully adult (Galatius & Kinze 2003; Moran *et al.* 2015). Cranial bones are thick and no cranial suture appears open. In addition, the filling of the anterior-most upper dental alveoli by greatly thickened bony pads, as well as the removal of the whole crown and part of the root through intense wear in one of the preserved teeth, may be considered indications of a relatively old individual (see below; Moore 1968; Kurihara *et al.* 2016). On the other hand, cross-sections of fragmented teeth of MUSM 2543 display a pulp cavity that is not completely filled with dentine. However, the pulp cavity remains open in adult specimens of the extant *Physeter macrocephalus* (e.g. Boschma 1938; Pierce & Kajimura 1980). Altogether, the features listed here suggest an adult, possibly relatively old, individual.

Cranium (Figs 2–11)

General cranial morphology. With a condylobasal length of about 1300 mm and a bizygomatic width of 505 mm (Table 1), *Rhaphicetus valenciae* MUSM 2543 represents a medium-sized physeteroid, with a cranium markedly larger than that of kogiids, slightly larger than those of specimens of *Acrophyseter* spp. and *Orycterocetus crocodilinus* and slightly smaller than in the holotypes of '*Aulophyseter*' *rionegrensis* and *Diaphorocetus poucheti*, but considerably smaller than those of *Aulophyseter morricei*, *Zygophyseter varolai* and, to a greater extent, *Albicetus oxymycterus*, *Livyatan mevillei* and *Physeter macrocephalus* (Kellogg 1927, 1965; Bianucci & Landini 2006; Boersma & Pyenson 2015; Velez-Juarbe *et al.* 2015; Lambert *et al.* 2017; Paolucci *et al.* 2020).

The robust and horizontal rostrum of MUSM 2543 is long (Figs 2, 4, 5, 14), representing about 75% of the condylobasal length. Such a proportion is in the upper range of adult male *Physeter macrocephalus*, higher than in kogiids, '*Aulophyseter*' *rionegrensis*, *Acrophyseter* spp., *L. melvillei*, *Z. varolai* and most likely *Idiorophus patagonicus*; the ratio between bizygomatic width and condylobasal length is estimated to be 0.39, lower than in *P. macrocephalus* (Flower 1867a; Lydekker 1893; Omura *et al.* 1962; Clarke & Paliza 1972; Velez-Juarbe *et al.* 2015; Lambert *et al.* 2017). It is important to note that the anterior part of the rostrum is often missing in fossil physeteroid skulls, making cranial proportions difficult to calculate (e.g. Kellogg 1927, 1965; Gondar 1975; Lambert 2008; Paolucci *et al.* 2020). The anterior part of the rostrum is narrow, with lateral margins that only slightly diverge posterolaterally for more than half its length. In this anterior portion, the rostrum was either as high as wide in cross-section (roughly cylindrical) or slightly higher than wide. In lateral view, the ventral region of the rostrum appears to be truncated in the apical region, with the ventral margin raising markedly anterodorsally. Observed on both sides, this unusual pattern seems to be a genuine anatomical feature, which may be correlated to the development of bony pads in dental alveoli of this region (see below).

Significant broadening of the rostrum occurs in its posterior third, towards the antorbital notches, as in many other extinct physeteroids (e.g. *A. morricei*, '*A.*' *rionegrensis*, *D. poucheti*, *O. crocodilinus*, *Physeterula dubusi*, *Placoziphius duboisi*, *Z. varolai* and *Acrophyseter* spp.); just anterior to the notches the rostrum is nearly 4.5 times wider than at midlength. The neurocranium is short and broad, roughly circular in dorsal view. Its dorsal surface is deeply excavated by a supracranial basin (Figs 2, 3, 6) that is proportionally narrow (compared, for example, to extant physeteroids, *Acrophyseter* spp., *L. melvillei*, *Z. varolai* and probably *Idiorophus patagonicus*), forming only 55% of the bizygomatic width. This value falls in the range of *O. crocodilinus*, which displays a marked variation in the breadth of the basin (Kellogg 1965), but it is smaller than in '*A.*' *rionegrensis*. Considering the dorsomedial slope of the dorsal surface of the premaxilla 100–120 mm anterior to the antorbital notch, it is proposed that the supracranial basin barely invaded the rostrum, a marked difference with *L. melvillei*, *P. macrocephalus*, *Aprixokogia kelloggi* and kogiine kogiids. The antorbital notches are located outside the basin, a plesiomorphic condition differing from kogiine kogiids. In the posterior part of the basin the bony nares are highly asymmetrical, the left being more than two times wider than the right. The dorsal part of the occipital shield and nuchal crest are broken into several

Figure 1. Locality and position along the stratigraphic section of the holotype of *Rhaphicetus valenciae* MUSM 2543. **A,** simplified map providing the position of the Chilcatay Formation localities Ullujaya and Zamaca (type locality of *R. valenciae*); **B,** location of the East Pisco Basin on the southern coast of Peru; **C,** simplified stratigraphic section of the Chilcatay and lower Pisco formations in Ullujaya; **D,** simplified stratigraphic section of the Chilcatay and Formation in Zamaca, showing the exact position of the holotype of *R. valenciae* in allomember Ct1, facies association Ct1a. Both sections include positions of ash layers dated with $^{40}Ar/^{39}Ar$ and of samples dated with $^{87}Sr/^{86}Sr$. Maps and sections modified from Bianucci *et al.* (2018b); Di Celma *et al.* (2018, 2019); Bosio *et al.* (2020b).

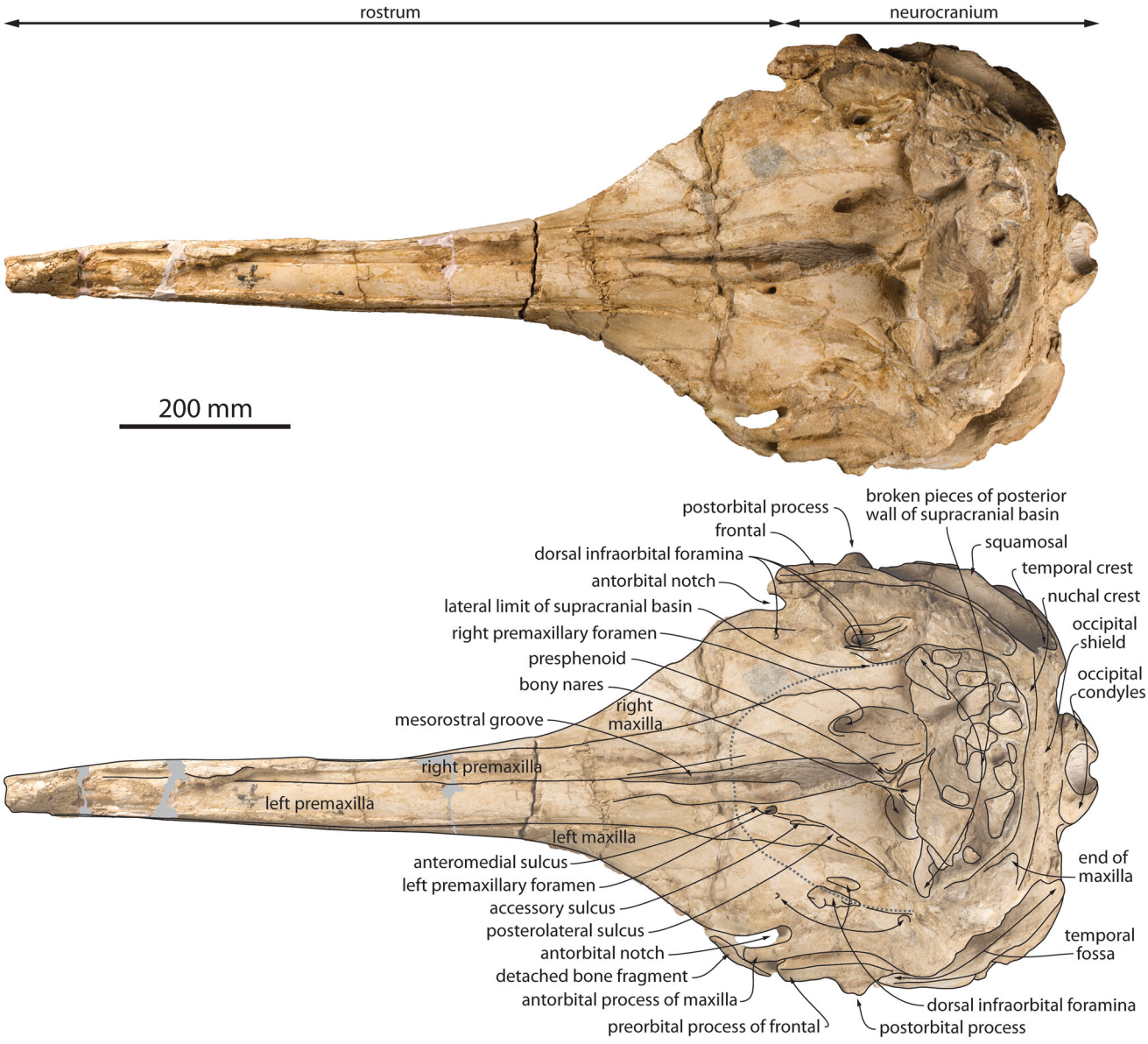

Figure 2. Cranium of *Rhaphicetus valenciae* MUSM 2543 (holotype) in dorsal view. Grey shading indicates main reconstructed parts; dotted grey line indicates approximate outline of the supracranial basin.

fragments, which collapsed in the posterior part of the supracranial basin; the dorsal extent of the posterior wall of the basin thus cannot be precisely estimated. However, based on the size of the main detached fragments and the section of the nuchal crest as preserved, the height of the crest above the occipital condyles probably did not exceed 120–130 mm. In lateral view (Figs 4, 5) the orbit is higher than the lateral margin of the rostrum (except for the posterior-most part of the rostrum, just before the antorbital notch), differing from the condition in kogiids, *A. morricei* and *P. macrocephalus*. The temporal fossa is anteroposteriorly elongated, about two times longer than the orbit, but proportionally only moderately dorsoventrally high (Table 1), originally significantly lower than the top of the nuchal crest. It is lower and longer than in *O. crocodilinus*, much longer than in *A. morricei* and *P. macrocephalus*, and lower than in *Acrophyseter* spp., being more similar to that of '*A.*' *rionegrensis*.

Premaxilla. Due to fractures in the anterior part of the rostrum and the loss of anterior fragments of the maxilla, the extent of the anterior premaxillary part of the rostrum cannot be estimated in MUSM 2543. Although

Table 1. Skull measurements (in mm) of *Rhaphicetus valenciae* gen. et sp. nov. MUSM 2543 (holotype). **Abbreviations: +**, incomplete; **e**, estimate.

Cranium	
Condylobasal length as preserved (tip of rostrum missing)	+1263
Reconstructed condylobasal length	e1308
Rostrum length as preserved	+910
Reconstructed rostrum length	e955
Width of rostrum at mid-length	84
Height of rostrum at mid-length (premaxillae dorsoventrally crushed)	+80
Width of rostrum at one-quarter length (from antorbital notch)	150
Height of rostrum at one-quarter length (premaxillae dorsoventrally crushed)	+90
Maximum width of rostrum just anterior to antorbital notches	374
Width of rostrum at base	376
Width across the two premaxillae at rostrum base	172
Transverse width of right premaxillary foramen	18
Transverse width of left premaxillary foramen	9
Width of right premaxilla at level of premaxillary foramen	85
Transverse width of right bony naris	18
Transverse width of left bony naris	38
Preorbital width	476
Postorbital width	507
Maximum width of supracranial basin (behind posterior dorsal infraorbital foramina)	278
Distance between level of antorbital notch and posteromedial wall of supracranial basin (nuchal crest)	250
Length of right orbit	103
Length of left orbit	97
Height of right postorbital process	76
Height of left postorbital process	76
Maximum length of right temporal fossa	212
Maximum length of left temporal fossa	195
Maximum height of right temporal fossa (taken vertically in posterior region)	92
Maximum height of left temporal fossa	91
Maximum transverse width of right temporal fossa from medial wall to mastoid crest	125
Bizygomatic width	505
Distance between medial margins of paroccipital processes	263
Distance between lateral margins of basioccipital crests	243
Distance between anterior tip of right zygomatic process (incomplete) and ventral tip of postglenoid process	+167
Width of occipital condyles	128
Height of right occipital condyle	78
Height of left occipital condyle	88
Height of foramen magnum	53
Minimum distance between temporal fossae across occipital shield	252
Right periotic	
Total length	40.0
Maximum mediolateral width	22.7
Maximum dorsoventral width	20.8
Length of anterior process	8.7
Maximum mediolateral width of anterior process with accessory ossicle	15.2
Maximum mediolateral width of anterior process without accessory ossicle	12.8
Maximum dorsoventral width of anterior process with accessory ossicle	12.0
Maximum mediolateral width of accessory ossicle with fragment of outer lip	8.7
Maximum anteroposterior length of accessory ossicle	e8.4
Length of pars cochlearis from anterior wall to anterior margin of fenestra rotunda	15.8
Maximum dorsoventral thickness of pars cochlearis from ventral wall to ventral margin of internal acoustic meatus	11.8
Length of posterior process	17.5
Maximum width of posterior bullar facet	e11.3
Left tympanic bulla	
Total length without posterior process	34.8
Maximum transverse width of posterior process as preserved	12.8
Anteroposterior length of accessory ossicle	8.7
Maximum mediolateral width of accessory ossicle	8.6

(*Continued*)

Table 1. Continued.

Left malleus	
Total height in posteromedial view	4.7
Height of largest facet for incus	3.1
Height of shortest facet for incus	2.2
Height of malleus to upper margin of largest facet	3.4
Maximum width across facets for incus	4.6
Left incus	
Total height	3.6
Maximum diameter of largest articular facet for malleus	3.6
Height of shortest articular facet for malleus	2.1
Mandible	
Preserved length of right mandible (incomplete)	830
Preserved length of mandibular symphysis (incomplete)	360
Height of mandible at posterior end of symphysis	63
Width of mandible at posterior end of symphysis	33
Height of mandible at anterior end of mandibular foramen	106

there are indications suggesting that the left maxilla did reach the preserved apex of the rostrum (possible traces of the premaxilla-maxilla suture on the poorly preserved lateral surface), the observation of a more abrupt descent of the premaxilla-maxilla suture on the right side suggests that the premaxillae alone occupied the first 70–80 mm of the rostrum (Figs 4, 5). More posteriorly the premaxilla-maxilla suture is clearly visible along the lateral surface of the rostrum; no lateral groove is observed along this suture. On the somewhat better preserved right side, the lateral surface of the premaxilla is marked by a series of narrow longitudinal sulci, some being directed anteriorly and others more anteroventrally, along the anterior-most 300 mm of the rostrum, indicating some degree of vascularization/innervation of the tip of the snout. The dorsomedial plate of each premaxilla is crushed in the mesorostral groove, with the left premaxilla covering the right. The exposed transverse width of the left premaxilla, its slightly transversely convex dorsal surface, and its rectilinear medial edge suggest that the mesorostral groove was originally dorsally closed by the premaxillae for most of its length (more so than in '*Aulophyseter*' *rionegrensis* and *Orycterocetus crocodilinus*, and probably more similar to *Aulophyseter morricei* and *Idiorophus patagonicus*), but the two premaxillae were most likely not sutured dorsomedially. Parts of the left and right premaxillae preserved in their original position indicate a moderate (20–30°) dorsomedial slope of the dorsal surface of these bones 120 to 100 mm anterior to the antorbital notch. As mentioned above, the supracranial basin was therefore limited to the neurocranium and the posteriormost part of the rostrum. From about 120 mm anterior to the notch, the medial margin of the right premaxilla diverges slightly posterolaterally; the mesorostral groove was therefore dorsally open from this level to the anterior margin of the bony nares (Figs 2, 3). As far as 200 mm anterior to the antorbital notch, the dorsal surface of the right premaxilla is transversely convex. From there, the lateral half of the surface becomes transversely concave, with the lateral edge rising posteriorly and slightly laterally. A long sulcus (at least 90 mm long) is observed along the medial margin of the right premaxilla in the region of the rostrum base, reaching posteriorly the level of the left premaxillary foramen; it is tentatively interpreted as the anteromedial sulcus. In dorsal view, the suture with the maxilla is slightly laterally convex at the level of the antorbital notch, diverging slightly posterolaterally up to the level of the right premaxillary foramen. The latter is located 50 mm posterior to the antorbital notch, a marked difference with, for example, '*A.*' *rionegrensis*, *Diaphorocetus poucheti* and *O. crocodilinus*, which are characterized by a right premaxillary foramen that is anterior to the notch. From that level, the premaxilla-maxilla suture takes a posterior direction and descends slightly posteroventrally along the lateral wall of the supracranial basin. The right premaxilla does not, therefore, cover the whole lateral wall of the supracranial basin, contrasting on that point, for instance, with *Acrophyseter* spp. The right premaxilla-maxilla suture diverges abruptly posterolaterally in some specimens of *O. crocodilinus*, in *Livyatan melvillei*, and in *Physeter macrocephalus*. The large right premaxillary foramen is followed posteriorly by a broad, deep, and well-defined sulcus. The latter widens transversely, with a vertical lateral wall and a convex lateral outline. Posteromedial to this sulcus the surface of the posteromedial corner of the right premaxilla is excavated by a shallow depression, at the level of the anterior margin of the

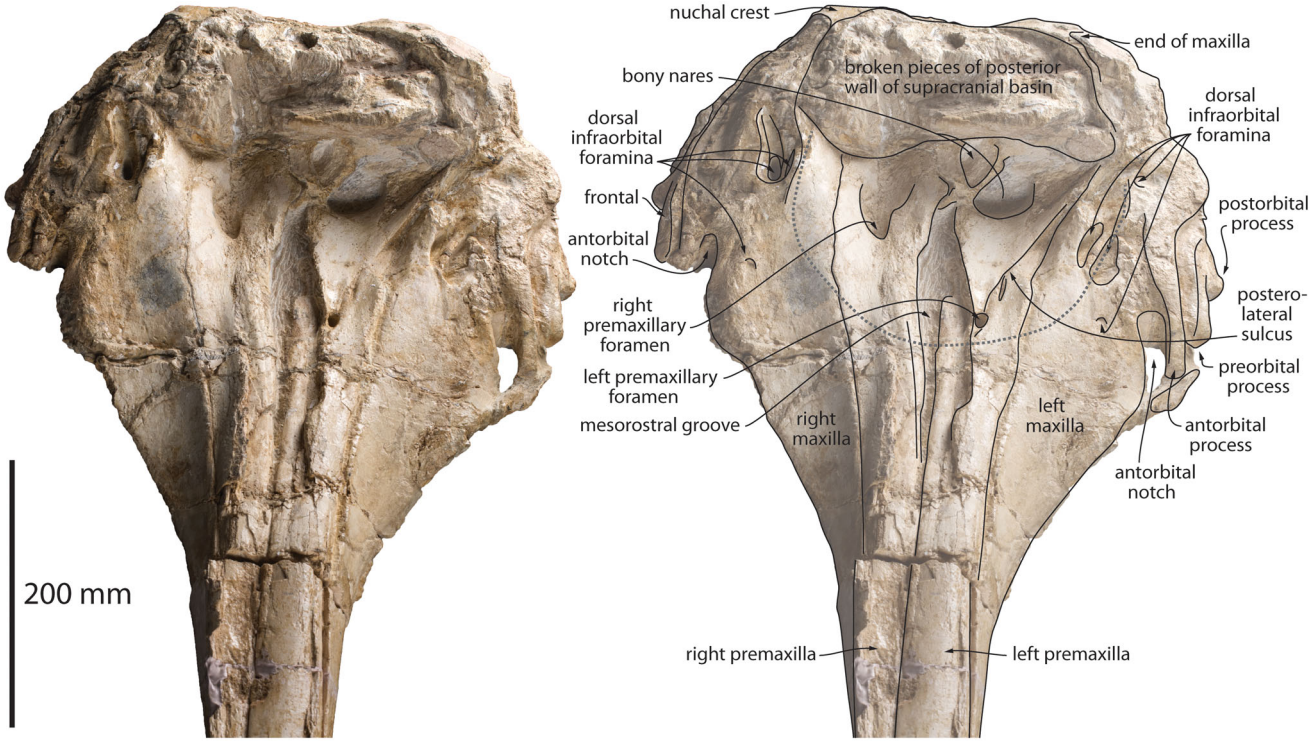

Figure 3. Neurocranium and proximal part of the rostrum of *Rhaphicetus valenciae* MUSM 2543 (holotype) in anterodorsal view. Dotted grey line indicates approximate outline of the supracranial basin.

bony nares. Separated from the rest of the bone by a fracture, a flat plate of the right premaxilla makes the medially concave lateral wall of the small right bony naris. In anterior view the floor of the latter is located significantly higher than the floor of the left bony naris, reaching a level that is at about mid-height of the left naris. The posterior-most part of the right premaxilla is hidden under detached fragments of the nuchal crest.

The left premaxillary foramen is located just anterior (16 mm) to the level of the antorbital notch (Figs 2, 3, 7A), 35 mm medial to the maxilla-premaxilla suture, and is much narrower than the right (Table 1). A short anteromedial sulcus is preserved for 20 mm. A narrow posterolateral sulcus leaves the foramen posteriorly and slightly laterally, turning gradually more laterally and rising towards the posterolateral corner of the supracranial basin. Medial to this sulcus the dorsal surface of the left premaxilla is transversely concave, with an elevated medial edge. This concave region, which widens markedly posteriorly, can reasonably be interpreted as a left premaxillary sac fossa. Its surface is smooth and flat to slightly anteroposteriorly convex. From the level of the posterior end of the mesorostral groove, the surface dives posteroventrally towards the floor of the large left bony naris. Lateral to the posterolateral sulcus, an anteroposteriorly extended sulcus exits the former sulcus anteriorly, for 26 mm. Posterolateral to this accessory sulcus, the surface of the premaxilla forms a marked depression that deepens and narrows posterolaterally along the posterolateral sulcus. In this region the lateral margin of the left premaxilla diverges posterolaterally up to a distance of 65 mm from the corresponding bony naris, and it contributes to the steep lateral wall of the supracranial basin. The latter forms an angle of about 45° with the horizontal. The posterior-most part of the left premaxilla is covered with detached fragments of the nuchal crest.

Maxilla. On the anterior part of the rostrum of MUSM 2543, the maxillae are not exposed dorsally; their lateral surface is nearly flat and sub-vertical (Fig. 2). The extent of this anterior portion is difficult to measure precisely, as the whole rostrum is slightly twisted clockwise, making the left maxilla more dorsally exposed than the right. From approximately the mid-length of the rostrum, the upper part of the lateral surface turns gradually dorsally and becomes transversely concave. In this region, the lateral edge of the rostrum forms a thin and flat lateral shelf and rises posterodorsolaterally towards the antorbital notch. This dorsoventrally flattened shelf widens posteriorly, with a conspicuously convex lateral edge, as, for instance, in *Aulophyseter*

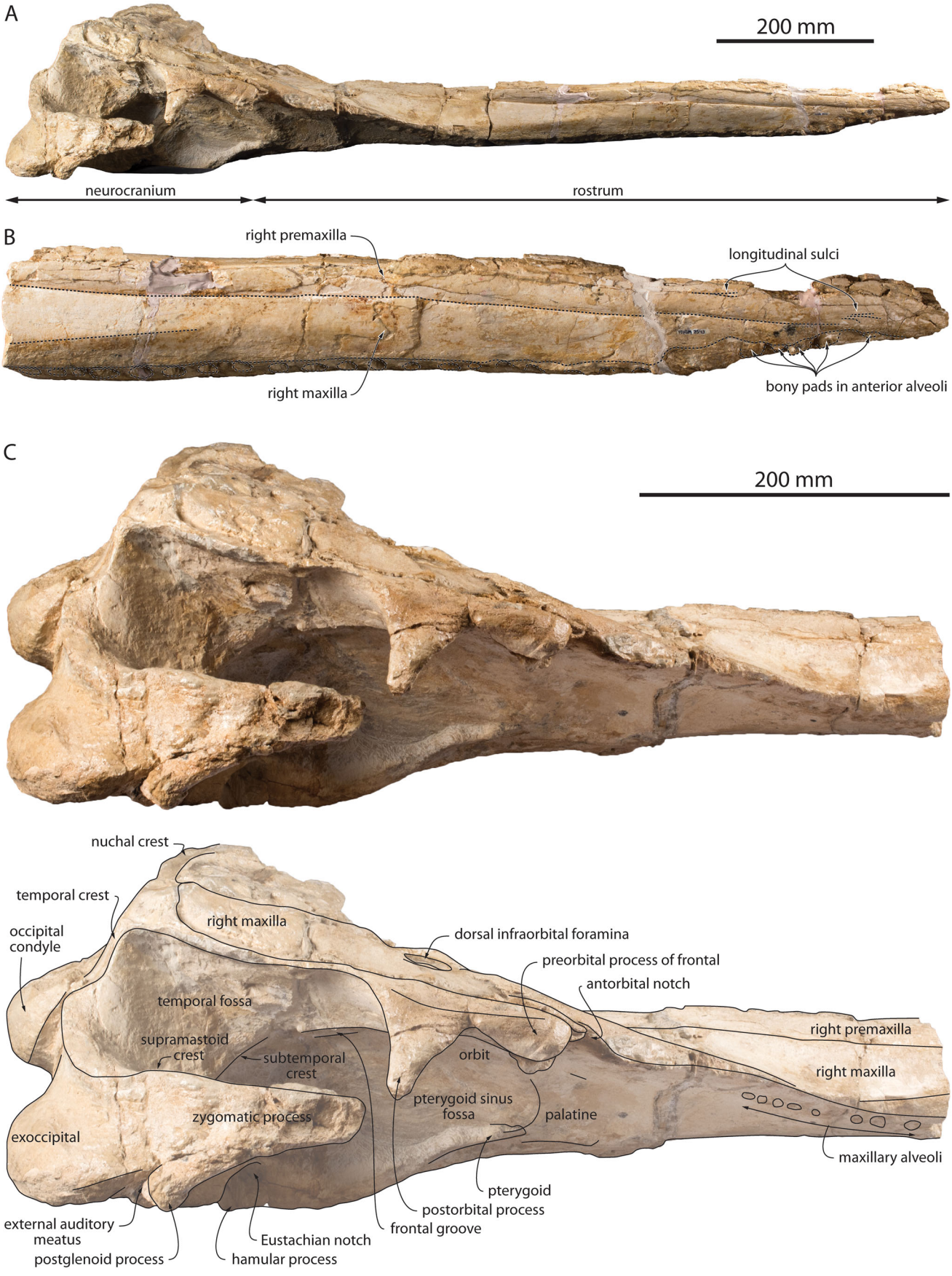
A
200 mm
neurocranium
rostrum
B
right premaxilla
longitudinal sulci
right maxilla
bony pads in anterior alveoli
C
200 mm
nuchal crest
temporal crest
occipital condyle
right maxilla
dorsal infraorbital foramina
preorbital process of frontal
antorbital notch
temporal fossa
supramastoid crest
subtemporal crest
orbit
right premaxilla
right maxilla
pterygoid sinus fossa
palatine
zygomatic process
exoccipital
maxillary alveoli
pterygoid
postorbital process
frontal groove
external auditory meatus
postglenoid process
Eustachian notch
hamular process

morricei, '*Aulophyseter*' *rionegrensis*, *Diaphorocetus poucheti*, *Orycterocetus crocodilinus*, *Physeterula dubusi* and most likely *Placoziphius duboisi*. The maximum width of the rostrum is located 80–90 mm anterior to the bottom of the antorbital notch, from where the lateral margins converge slightly towards their respective antorbital notches. At this widest point, this thin shelf slopes ventrolaterally. The lateral edge of the rostrum only thickens significantly dorsoventrally along the last 35 mm before the antorbital notch (Figs 4, 5).

At the level of the antorbital notch, the maxilla is considerably wider than the premaxilla in dorsal view (Figs 2, 3, 7A). Anteromedial to the antorbital notch, the broad dorsal surface of the right maxilla is transversely and anteroposteriorly concave, making a shallow depression. A tiny dorsal infraorbital foramen (transverse diameter 7 mm) is present 40 mm anteromedial to the antorbital notch. Two larger, anteroposteriorly elongated foramina are located posteriorly. The medial foramen is 35 mm × 5 mm, possibly including two subdivisions, and the lateral foramen is 25 mm × 12 mm. They are both found outside the supracranial basin, located in a single larger fossa (30 mm wide). The lateral foramen is followed posteriorly by a sulcus turning slightly posterolaterally. Medial to these foramina, the lateral wall of the supracranial basin is more vertical (about 60°) than on the left side, and, as mentioned above, only partly covered by the premaxilla. The position of the main dorsal infraorbital foramina is more posterior in *Rhaphicetus valenciae* than in many other physeteroids, including *Acrophyseter* spp., *Aulophyseter morricei*, '*Aulophyseter*' *rionegrensis*, *Eudelphis mortezelensis*, *Livyatan melvillei*, *Orycterocetus crocodilinus*, *Physeterula dubusi*, *Placoziphius duboisi* and *Zygophyseter varolai*.

Differing from the right side, the dorsal surface of the left maxilla is roughly flat and slopes anteriorly and slightly laterally at the base of the rostrum. Similar to the right side, a tiny dorsal infraorbital foramen, with a transverse diameter of 4.5 mm, is located 31 mm medial to the left antorbital notch (Figs 2, 3). Posteromedial to the notch, two large dorsal infraorbital foramina pierce the left maxilla; both are considerably anteroposteriorly elongated (59 mm × 17 mm for the lateral foramen and 42 mm × 11.5 mm for the medial foramen), with the medial foramen slightly more posterior. The lateral foramen anteriorly follows the lateral margin of the posterior part of the supracranial basin, thus indicating that at least the medial foramen can be identified inside the basin (a condition differing from the right maxilla), in a region where the basin's lateral extent is poorly defined. A smaller posterior dorsal infraorbital foramen (diameter of 13 mm) is located 50 mm posterolateral to the two large dorsal infraorbital foramina, opening laterally and slightly posteriorly.

Nearly completely lost on the right side, the antorbital process of the maxilla is finely preserved on the left side. In dorsal view, it is a finger-like, elongated process, pointing anteroventrally, extending 48 mm anterior to the bottom of the antorbital notch and 39 mm anterior to the preorbital process of the frontal, laterally defining a deep (45 mm) and relatively narrow (17–20 mm), 'U'-shaped antorbital notch that opens anteriorly and slightly laterally (Fig. 2). In lateral view the antorbital process is broadly exposed anterior to the preorbital process of the frontal, being dorsoventrally thick (Fig. 5). The prominent dorsomedial edge of the antorbital process runs posteriorly with a slight medial component, making a shallow crest between the main lateral dorsal infraorbital foramen and the lateral margin of the maxilla. In dorsal view the latter margin is concave in the supraorbital region, turning posterolaterally beyond the postorbital process before rising posterodorsomedially towards the nuchal crest. Along the thick lateral portion of the nuchal crest, each maxilla reaches only slightly beyond the level of the posteromedial wall of the temporal fossa (Figs 2, 3, 7A), remaining much more distant from the sagittal plane than, for instance, in *O. crocodilinus*, and being closer to the condition of '*Aulophyseter*' *rionegrensis*.

In ventral view, although the posterior-most maxillary alveoli are difficult to detect, being partly covered by hardened sediment, it can be observed that the alveolar row reached a level 143 mm anterior to the antorbital notch, maybe slightly less (Fig. 6). The last posterior alveoli detected are distant from the lateral margin of the rostrum (33 mm on the right side). From their posterior end the alveolar rows converge markedly anteromedially for about 300 mm, before forming a more gradual convergence, drawing a deeply laterally concave line in ventral view. The minimum upper tooth count is estimated to be 36 on the left side and 34 on the right, among which several alveoli may correspond to premaxillary teeth (see above). Although the upper tooth count is not precisely known in each species, such a count is considerably higher than in *Acrophyseter* spp., '*A.*' *rionegrensis*, *Brygmophyseter shigensis*, *Diaphorocetus poucheti*, *E. mortezelensis*, *L. melvillei*, *O. crocodilinus*,

Figure 4. Cranium of *Rhaphicetus valenciae* MUSM 2543 (holotype) in right lateral view. **A,** whole cranium; **B,** distal part of the rostrum; **C,** neurocranium and proximal part of the rostrum.

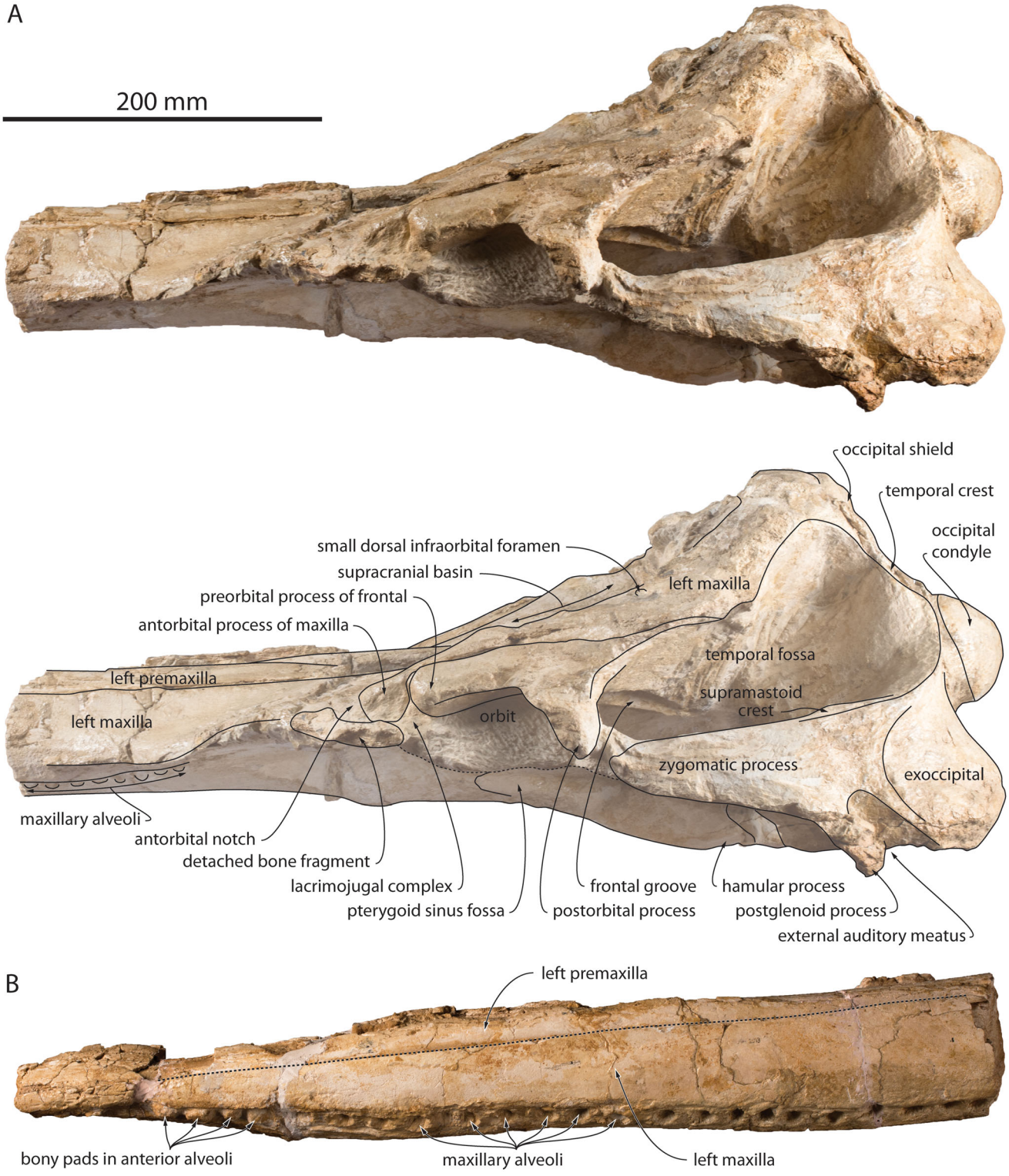

Figure 5. Cranium of *Rhaphicetus valenciae* MUSM 2543 (holotype) in left lateral view. **A,** neurocranium and proximal part of the rostrum; **B,** distal part of the rostrum.

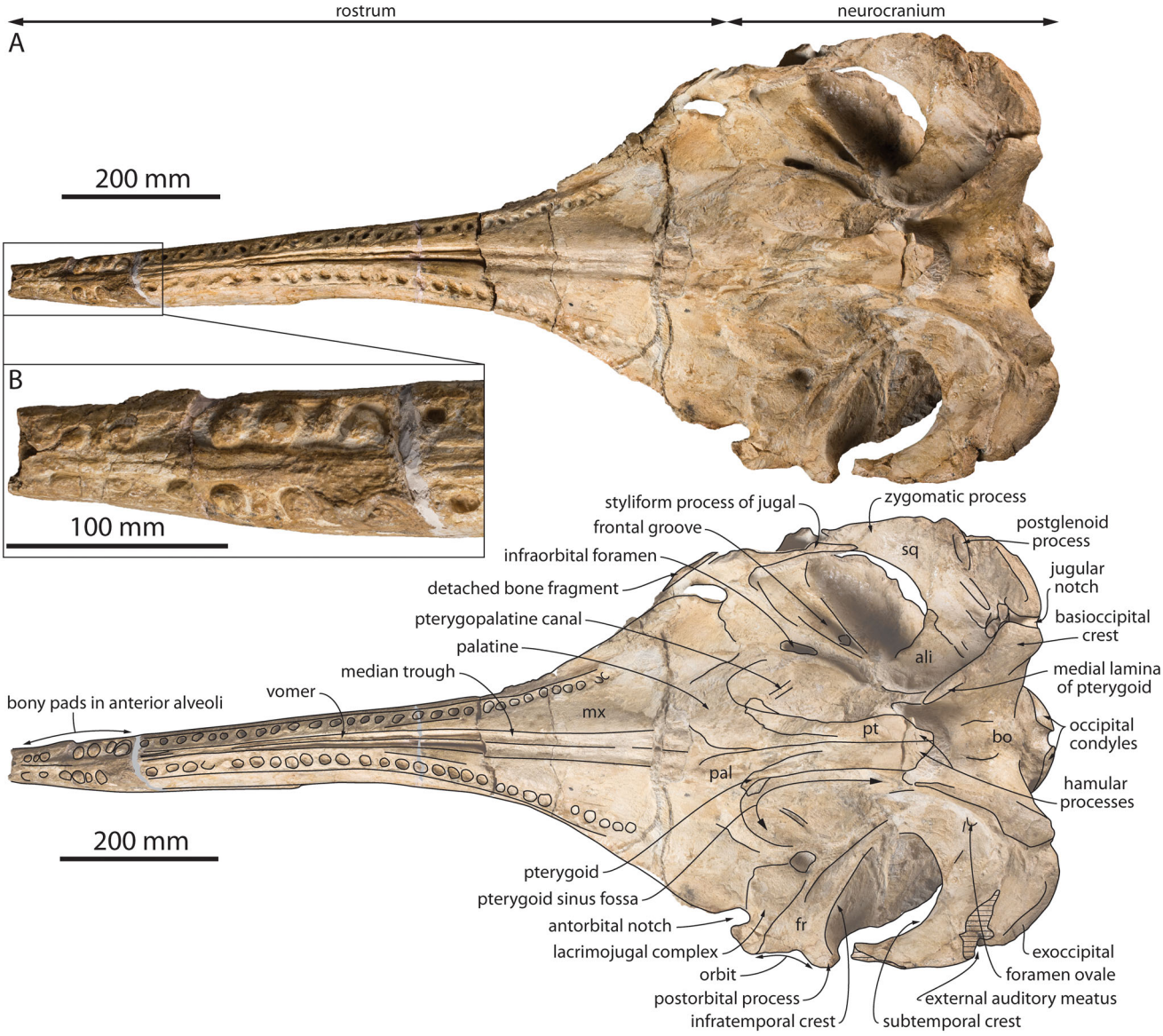

Figure 6. Cranium of *Rhaphicetus valenciae* MUSM 2543 (holotype) in ventral view. **A,** whole cranium; **B,** detail of the distal part of the rostrum. Grey shading indicates main reconstructed parts.

P. dubusi, *Z. varolai* and most likely *Ferecetotherium kelloggi*, and even higher than the mandibular tooth count of *Physeter macrocephalus*. Alveoli open ventrally and slightly laterally. Posterior alveoli range in transverse diameter between 9 and 14 mm. Alveolar diameter decreases slightly forward, down to 9.5–10.5 mm. Interalveolar septa display irregular thicknesses, ranging from 3 to 12 mm, with a trend for thicker septa in the anterior part of the rostrum. Along the anterior 170 mm of the rostrum, the alveoli of MUSM 2543 are surprisingly filled with large bony pads, made of spongy bone (Fig. 6B). These pads protrude from the corresponding alveoli and display somewhat irregular outlines and sizes. At least five bony pads are counted on both sides, with diameters up to 18.5 mm; anterior pads are significantly smaller, the first left pad having a transverse diameter of 8 mm. These bony pads are strongly reminiscent of pads observed in alveoli of some extinct and extant ziphiids (e.g. mandibular alveoli of Ziphiidae indet. IRSNB M.538 and IRSNB 3855, from the Neogene of Antwerp; in mandibular alveoli of *Ninoziphius platyrostris*, from the late Miocene of the Pisco Basin; in maxillary alveoli of *Tasmacetus shepherdi*; and in apical mandibular alveoli of *Berardius* spp. and *Ziphius cavirostris*: OL pers. obs.; True 1910; Moore 1968; Muizon 1984;

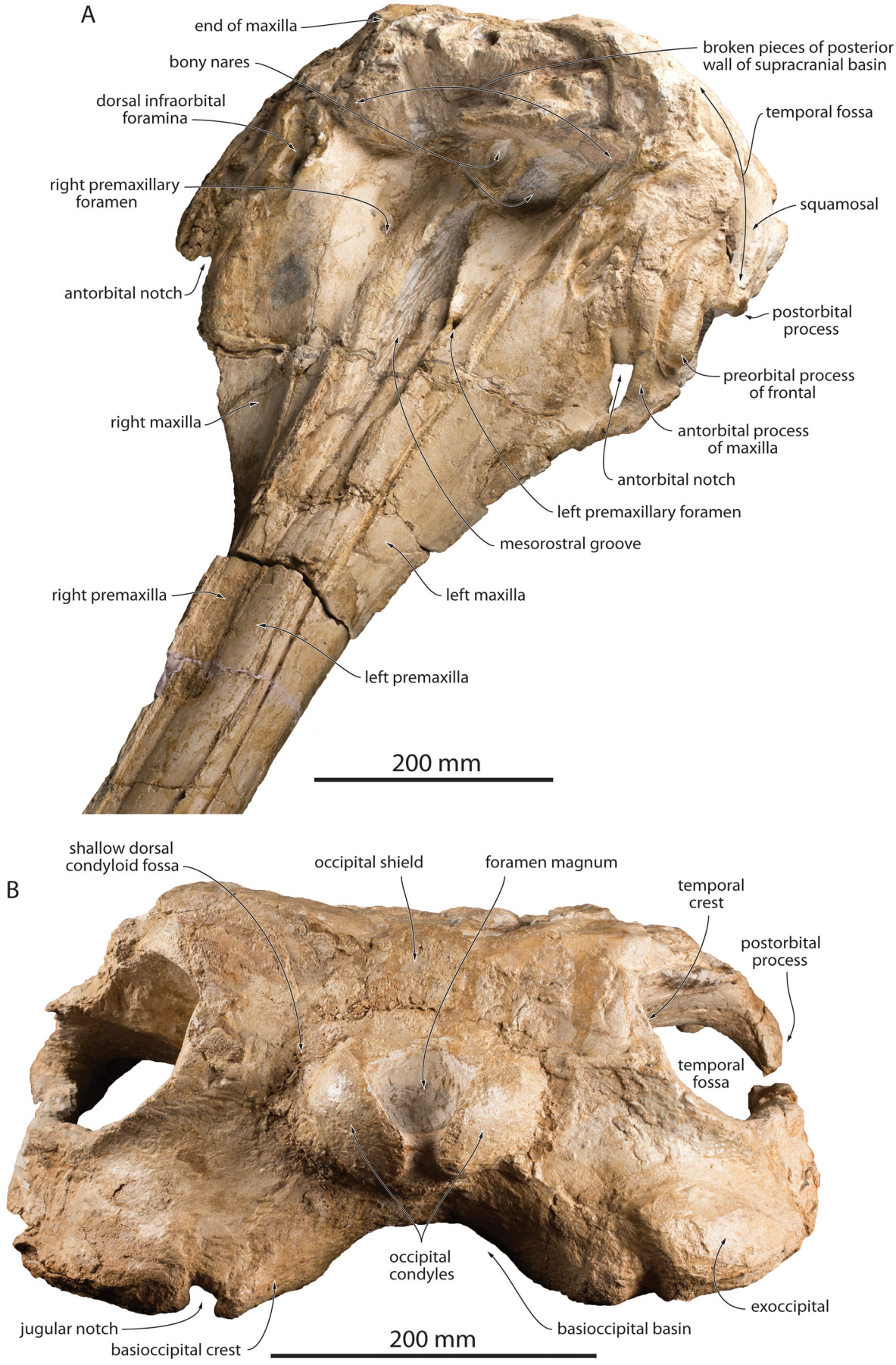

Figure 7. Cranium of *Rhaphicetus valenciae* MUSM 2543 (holotype) in **A,** left anterodorsolateral and **B,** posterior views.

Lambert 2005a). Interestingly a similar feature has been observed in the extant delphinid *Peponocephala electra*, with posterior alveoli gradually filled with bony tissue through ontogeny, a process leading to tooth loss and the formation of a convex bony pad (Kurihara *et al.* 2016).

Between the alveolar rows, a deep median trough extends for most of the rostrum length (Fig. 6). It shallows and narrows anteriorly, and it becomes barely visible 200 mm from the anterior apex. Posteriorly, the trough reaches a maximum width of 26 mm, which is retained while shallowing backwards, until the trough disappears a short distance anterior to the tip of the palatines. Medial to the last posterior alveoli, the ventral surface of each maxilla is transversely concave; this concave region widens posterolaterally as far as the level of the antorbital notch.

Presphenoid. A small piece of bone at the posterior end of the mesorostral groove is interpreted as a part of the presphenoid, wedged between right (above) and left (under) premaxillae, and joining the nasal septum posteriorly (Figs 2, 3, 7A). The latter slopes at about 50° from the horizontal, in relation with the higher position of the right bony naris, and it thickens dorsolaterally towards the left side of the supracranial basin.

Vomer. The vomer appears as a narrow keel in the median trough along the ventral surface of the rostrum (Fig. 6), as in *Orycterocetus crocodilinus*, starting posteriorly at about the level of the last alveolus and gradually rising forwards for at least 530 mm, being possibly replaced anteriorly by a ventromedial exposure of the premaxillae. The ventral exposure of the vomer is considerably wider, for instance, in the following taxa: *Acrophyseter deinodon*, '*Aulophyseter*' *rionegrensis*, *Eudelphis mortezelensis*, *Livyatan melvillei* and probably *Diaphorocetus poucheti*.

Palatine. On the broad, robust palate, the palatine-maxilla suture is partly visible on both sides (Figs 6, 8A). Medially, it first runs anteriorly before diverging markedly anterolaterally and laterally. The anterior tip of each palatine reached a level approximately 60 mm anterior to the antorbital notch. The lateral palatine-maxilla suture runs posterolaterally towards the anterior margin of the infraorbital foramen. Each palatine is crossed by a broad and shallow crest that turns laterally and posterolaterally. It is interpreted as the anterior limit of a large pterygoid sinus fossa (see for example Fraser & Purves, 1960, pl. 16 for the condition of the sinus in *Kogia breviceps*). In the centre of each fossa an oblique, anteromedially directed deep sulcus most likely corresponds to the artificially open canal leading to the major palatine foramen (= pterygopalatine canal).

Pterygoid. Anteriorly, each pterygoid is only preserved as a small scale of bone on the anteromedial region of the pterygoid sinus fossa, leading to a narrow strip of bone that gradually thickens transversely and dorsoventrally in a posteroventral direction, towards the hamular process of the pterygoid (Figs 6, 8A). This thick medial lamina of the pterygoid only partly ventrally covers the pterygoid sinus fossa. Posterior apices of the right and left hamular processes are joined medially, together reaching a level posterior to the Eustachian notch. This condition differs markedly from that of *Acrophyseter robustus*, *Aulophyseter morricei*, *Kogia* spp., *Orycterocetus crocodilinus*, *Physeter macrocephalus* and probably *Acrophyseter deinodon* (apices diverging posterolaterally), and to a lesser extent *Aulophyseter*' *rionegrensis* (nearly transversely directed posterior edge of each process), and is possibly more similar to that of *Eudelphis mortezelensis* (see Lambert 2008, fig. 4). Posterior to the Eustachian notch the medial lamina of the pterygoid forms a narrow crest (6–7 mm thick), which gradually thickens posterolaterally along the basioccipital basin. A shallow depression at about mid-length of the basin, on the ventral edge of the crest, is interpreted as the suture between pterygoid and basioccipital.

Lacrimojugal complex. In lateral view the lacrimojugal complex sends a thin, blade-like projection between the antorbital process of the maxilla and the preorbital process of the frontal (Fig. 5A). This projection is much smaller than that of several kogiids (e.g. *Kogia*, *Praekogia* and *Scaphokogia*). In ventral view, the lacrimal-frontal suture is distinct on the left side (Figs 6, 8A), oblique and rectilinear from the space between the infraorbital foramen and the frontal groove to the ventral tip of the preorbital process of the frontal. Better preserved on the left side (although partly hidden laterally by a detached, indeterminate bone fragment and sediment), the lacrimojugal forms a high (about 50 mm), sub-vertical and oblique plate located below the antorbital process of the maxilla and anterior to the preorbital process of the frontal, not differing significantly in this area from, for instance, *Acrophyseter robustus*, '*Aulophyseter*' *rionegrensis*, *Livyatan melvillei* and *Zygophyseter varolai*. Together with the antorbital process of the maxilla, but to a greater extent, it contributes to the lateral wall of the dorsoventrally deep antorbital notch. Only the dorsal part of the styliform process of the jugal is preserved (also on the left side), with a minimum anterior transverse width of 17 mm. This process reaches the zygomatic process of the squamosal and contacts its medial surface for at least 40 mm.

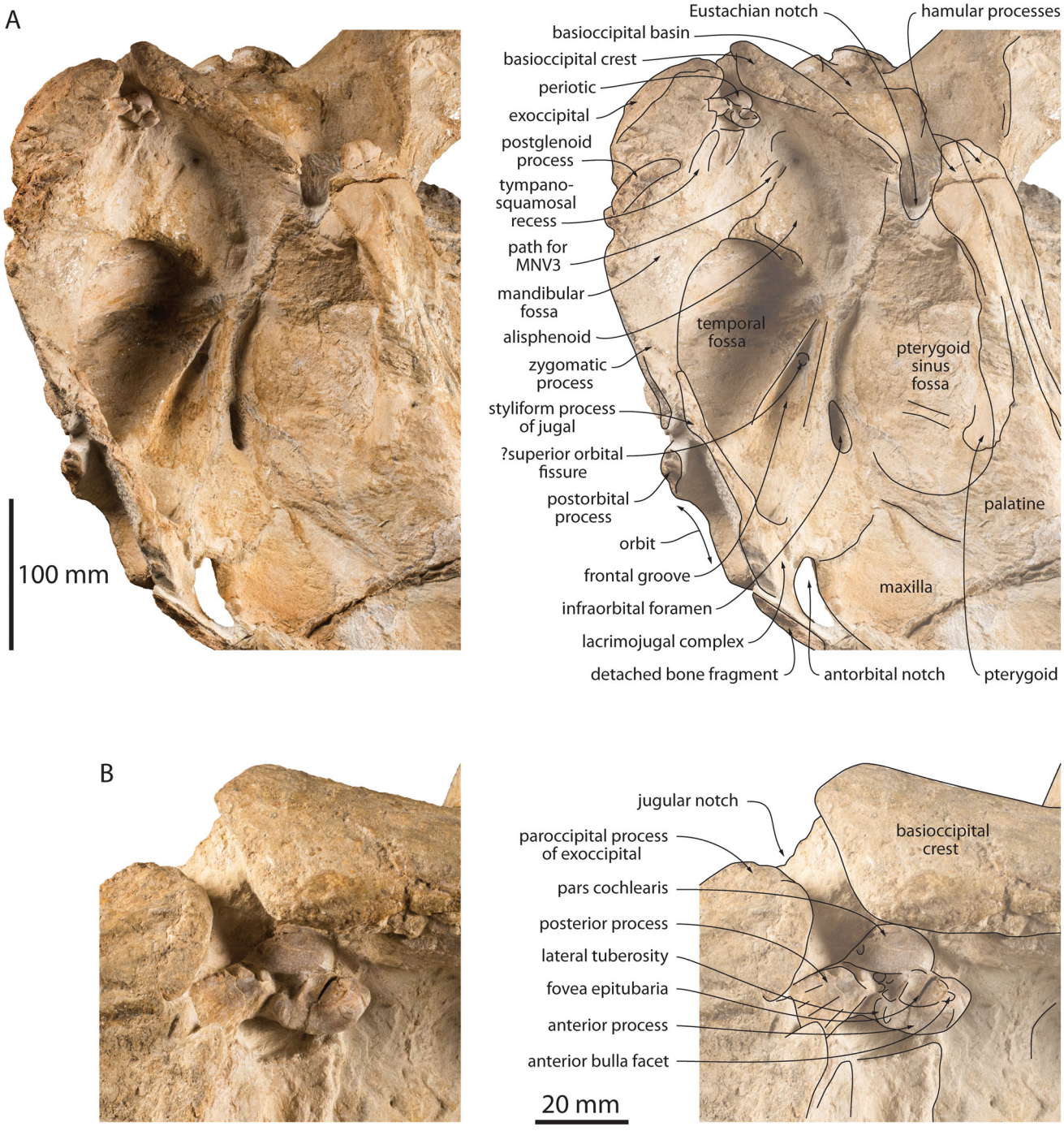

Figure 8. Detail of the basicranium of *Rhaphicetus valenciae* MUSM 2543 (holotype) in **A,** left anteroventrolateral view and **B,** detail of the posterior region showing the slightly anteromedially shifted left periotic.

Frontal. In lateral view the robust preorbital process of the frontal is not significantly dorsoventrally thickened (30 mm) as compared to the more posterior part of the bone (Figs 4, 5). The supraorbital process of the frontal only slopes slightly posterodorsally; the suture with the maxilla above the orbit makes an angle of 10–15° with the horizontal, which is significantly less than in many other physeteroids, including *Acrophyseter* spp., *Aulophyseter morricei*, '*Aulophyseter*' *rionegrensis*, *Orycterocetus crocodilinus*, *Zygophyseter varolai* and most kogiids. In dorsal view, the outline of the lateral margin of the supraorbital process is slightly concave

(more conspicuous on the left side; Fig. 2). Combined with the laterally projected postorbital process this condition results in orbits being somewhat dorsally open. In lateral view of the orbit, the ventral margin of the frontal forms an angle between its sub-horizontal upper part and the anterior margin of the postorbital process. This condition departs from the more regularly rounded outline of the orbit seen, for example, in kogiids, *A. morricei*, *Physeter macrocephalus* and *Z. varolai*, being more similar to the orbit of '*A.*' *rionegrensis*, *O. crocodilinus* and the large delphinid *Orcinus orca*. The long and robust postorbital process is moderately directed posteriorly.

In ventral view, the frontal groove is long, deep and obliquely directed (Figs 6, 8A); it is well defined posteriorly by the high infratemporal crest. Slightly lower at the base of the postorbital process, this crest is distinct along the medial wall of the process, giving it a triangular cross-section. A large foramen (diameter = 10 mm) could be detected in the frontal groove, 138 mm medial to the postorbital process. Although positioned at some distance from the medial end of the groove it could correspond to the superior orbital fissure. Also elevated, the anterior wall of the frontal groove separates the latter from a medium-sized infraorbital foramen. This foramen is sub-circular on the right side (27 by 24 mm) and more elongated on the left side (42 by 12 mm).

Supraoccipital. The preserved lower part of the occipital shield only rises for about 60 mm above the occipital condyles (Figs 3, 7B). Its surface is roughly flat, only slightly concave dorsomedial to the temporal crests. In lateral view its preserved surface forms an angle of 50–60° with the horizontal (Figs 4, 5). The thick temporal crest only protrudes posterolaterally in its lower half, before turning lateroventrally to join the thick supramastoid crest.

Squamosal. The anterior part of the much elongated and sub-horizontal zygomatic process of the squamosal is a transversely thin, vertical plate that does not contact the postorbital process of the frontal (Figs 4, 5, 14). Among physeteroids, the zygomatic process is longer (and more slender) only in *Zygophyseter varolai*; the length and proportions of the process in MUSM 2543 are close to those of '*Aulophyseter*' *rionegrensis*. The dorsal edge of the process rises gradually posterodorsally and is rectilinear for most of its length, the transversely thick supramastoid crest only bulging slightly dorsally at the anteroposterior level of the postglenoid process. This condition is similar to that of *Aprixokogia kelloggi* and *Praekogia cedrosensis*, but contrasts with that of many other physeteroids (e.g. *Acrophyseter deinodon*, *Aulophyseter morricei*, '*Aulophyseter*' *rionegrensis*, *Diaphorocetus poucheti*, *Kogia* spp., *Livyatan melvillei*, *Orycterocetus crocodilinus*, *Physeter macrocephalus* and *Z. varolai*), in which the supramastoid crest rises more abruptly posterodorsally before the level of the postglenoid process (see Bianucci & Landini 2006, fig. 12; Velez-Juarbe *et al.* 2015). Medial to the supramastoid crest, the floor of the broad squamosal fossa is anteroposteriorly and transversely concave. The ventral edge of the zygomatic process is slightly convex in its anterior portion.

Whereas the external auditory meatus is partly preserved on both sides, the postglenoid process is better preserved on the left side (Fig. 5). It is a nearly transversely directed robust bar, 15 mm thick at mid-length, and extending for 22 mm ventral to the external auditory meatus, thus being proportionally shorter than in *Eudelphis mortezelensis* but somewhat better defined than in *P. macrocephalus*, closer to the condition in '*Aulophyseter*' *rionegrensis*. Between the postglenoid process and the anterolateral part of the exoccipital, the posttympanic process of the squamosal is short (20–25 mm long ventral portion).

The mandibular fossa is transversely broad (about 55 mm, being poorly defined medially), transversely flat, moderately anteroposteriorly concave and facing anteroventrally (Figs 6A, 8A). The tympanosquamosal recess is better defined posteromedial to the postglenoid process, forming a triangular, narrow fossa pointing towards the lateral tuberosity of the periotic (preserved *in situ* on the left side). No evidence for the presence of a deep oblique groove medial to the tympanosquamosal recess, as observed in *Acrophyseter* spp., could be found. No remains of the falciform process could be detected. Best seen on the right side, the foramen ovale has a diameter of 12 mm, opening anterolaterally. It is followed by a shallow path for the mandibular nerve V_3, directed towards the anterior margin of the squamosal fossa (posterior-most part of the subtemporal crest).

Exoccipital. The jugular notch is wide (10 mm on the left side; Figs 7B, 8). The paroccipital process of the exoccipital is massive, as for the rest of the ventral margin of the bone, with the anteroposterior thickness of this margin exceeding 30 mm. The posterior surface of the exoccipital is dorsoventrally concave and it turns markedly anterolaterally, reaching a level anterior to the posterior wall of the temporal fossa (best seen on the left side). Although preceded by a relatively short (less than 10 mm) condylar neck, the large occipital condyles are strongly protruding, located high along the posterior wall of the neurocranium (ventral margin as high as the dorsal edge of the supramastoid crest on the squamosal), and with their articular surfaces facing posterodorsally (forming an angle of nearly 30° with the horizontal; Figs 4, 5, 14). As a consequence of this orientation, the

cranium most likely created an angle with the vertebral column in lateral view, with the rostrum pointing considerably upwards. A similar condition is observed in *Orycterocetus crocodilinus*, and the opposite pattern (with the rostrum pointing downwards) is observed in *Kogia* spp. and *Physeter macrocephalus*. A shallow depression corresponding to the dorsal condyloid fossa is found dorsolateral to each condyle.

Basioccipital. From the pterygoid-basioccipital suture the basioccipital crest expands considerably posterolaterally, making a robust flange that partly covers the pars cochlearis of the likely slightly dislocated left periotic in ventral view (Figs 6, 8). No carotid foramen could be detected along the lateral surface of the basioccipital crest, this area remaining hidden under a thin layer of hard sediment. Defined by the basioccipital crests, the basioccipital basin (*sensu* Muizon 1991) is proportionally anteroposteriorly short (distance between the Eustachian notch and posterolateral tip of the basioccipital crest = 148 mm), deep and broadly open posteroventrally (the basioccipital crests form an angle of more than 90° in ventral view). The floor of the basin is saddle-shaped, transversely concave and markedly anteroposteriorly convex, abruptly sloping towards the choanae, similar to the condition in *Aulophyseter morricei*, '*Aulophyseter*' *rionegrensis*, *Orycterocetus crocodilinus* and *Physeter macrocephalus*, and differing from, for example, *Acrophyseter* spp. and *Kogia* spp., which display a roughly anteroposteriorly flat, long basioccipital basin.

Alisphenoid. The alisphenoid-squamosal suture is partly visible on the left side, roughly following the anterior margin of the path for the mandibular nerve V_3 (Figs 6, 8A). The ventral surface of the alisphenoid is flat to slightly convex, rising anterodorsally towards the region of the orbital fissures.

Periotic. The complete left periotic is held *in situ* in the basicranium of MUSM 2543 (see Fig. 8). It most likely shifted slightly medially and dorsally from its original position, as it appears closely appressed to the lateral wall of the basioccipital crest, too dorsal compared to the level of the external auditory meatus, and directed anteromedially.

Detached from the basicranium, the right periotic is finely preserved and nearly complete, with only minor damage along the anteromedial angle and the outline of the posterior bullar facet (Fig. 9). The description below is based on the right periotic. This bone is proportionally small, with a short anterior process and a moderately inflated, low pars cochlearis (Table 1), similar to, for example, an isolated physeteroid periotic from the late early to early middle Miocene of Malta (Bianucci *et al.* 2011); it is distinctly smaller and more slender than the periotic of the otherwise smaller stem physeteroid *Acrophyseter deinodon*. The ventral surface of the anterior process displays a broad and long fovea epitubaria, housing the large accessory ossicle of the tympanic, a feature typical for physeteroids (see Bianucci & Landini 2006; Lambert *et al.* 2017), but also for the heterodont odontocete *Inticetus vertizi* (Lambert *et al.* 2018). As in the latter, and in several physeteroids, the tip of the anterior bullar facet is exposed anterior to the accessory ossicle, for 3 mm, with a slightly transversely concave surface. The ventral surface of the accessory ossicle bears fine longitudinal striations that may correspond to the origin of the tensor tympani muscle, as proposed for the delphinid *Tursiops* (Mead & Fordyce 2009). The anterior process has the three-spined morphology observed in kogiids (Muizon 1988; Vélez-Juarbe *et al.* 2016), with anteroventral, anterodorsal and dorsal spines. In kogiids these structures are generally relatively sharp and pointed (except for the dorsal spine, which is generally distinctly tubercle-like rather than pointed), which justifies the term 'spine' used by previous authors. However, in non-kogiid physeteroids their morphology is different. Although the anteroventral spine is sharp, the other two are either rounded and massive (anterodorsal spine) or ridge-like (dorsal spine). We retain the term 'spine' for these structures, although it is not morphologically coherent in some cases. The anteroventral spine bears the small anterior bullar facet and projects distinctly ventrally. Dorsal to this spine and anterodorsal to the accessory ossicle is a massive and tubercle-like anterodorsal spine. It projects anteriorly slightly beyond the tip of the anteroventral spine. The anterodorsal spine has a slightly damaged surface and may have been more pointed originally, as in some kogiids for example. It is less voluminous than in *A. deinodon*. The anteroventral and anterodorsal spines are separated by a slight longitudinal depression. On the dorsal aspect of the anterior process is the ridge-like dorsal spine. Medial to this ridge and posterior to the anterodorsal spine is a small anteromedially facing cupula. The crest of the dorsal spine extends posteriorly along the lateral edge of the pars cochlearis and reaches the dorsal process posteriorly. In fact, the ridge-like dorsal spine of the anterior process may be part of the residual dorsal process (superior process of Kellogg 1936), which represents the attachment structure of the periotic to the squamosal.

The ventral edge of the anterior process bears on its lateral side a wide and low ridge, strongly concave medially, which is bordered medially by an elongated shallow groove, along the lateral edge of the accessory ossicle. At the posterior end of this ridge is a poorly

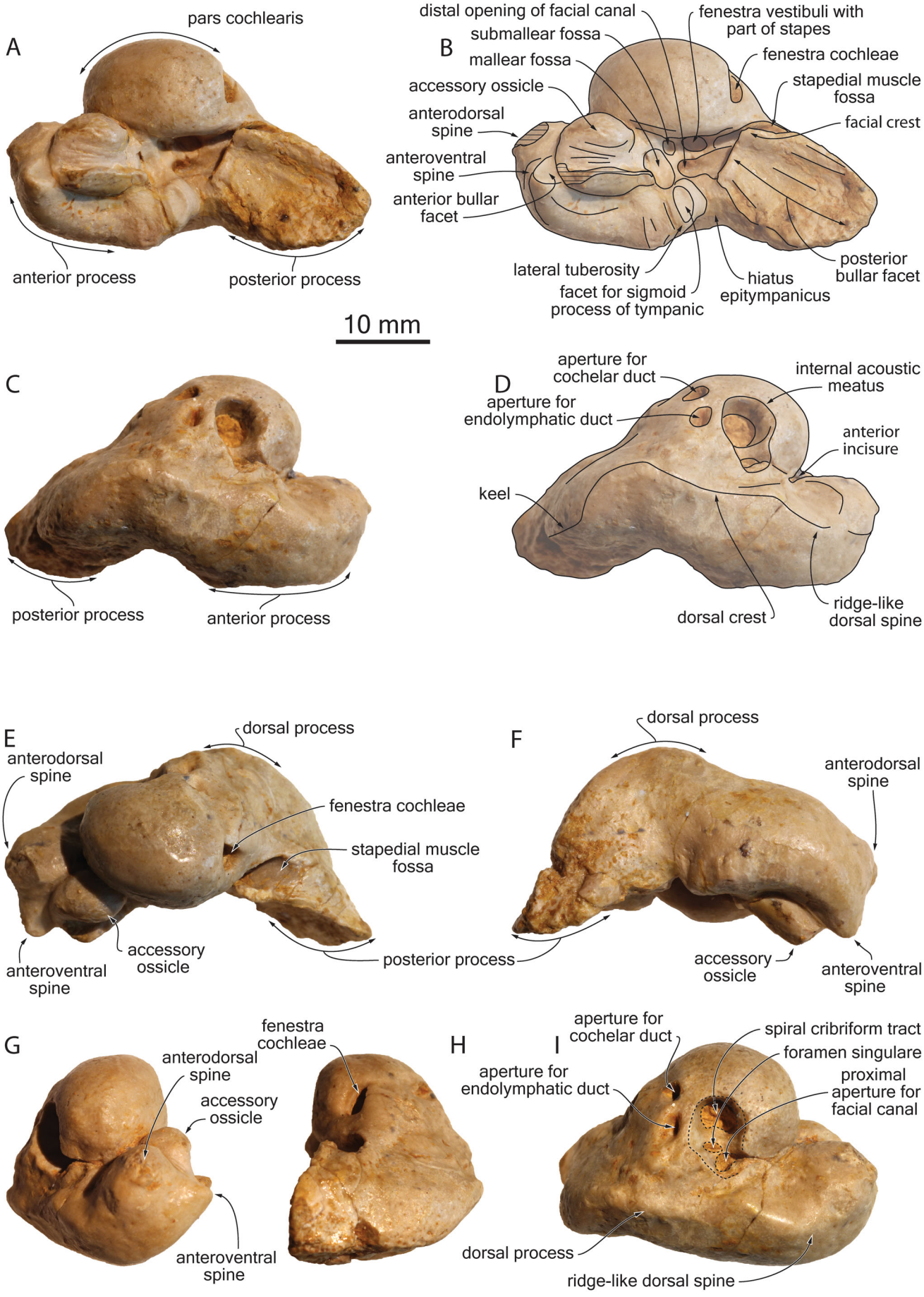
A
pars cochlearis
anterior process
posterior process
B
distal opening of facial canal
submallear fossa
mallear fossa
accessory ossicle
anterodorsal spine
anteroventral spine
anterior bullar facet
fenestra vestibuli with part of stapes
fenestra cochleae
stapedial muscle fossa
facial crest
posterior bullar facet
hiatus epitympanicus
lateral tuberosity
facet for sigmoid process of tympanic
10 mm
C
posterior process
anterior process
D
aperture for cochelar duct
aperture for endolymphatic duct
internal acoustic meatus
anterior incisure
keel
dorsal crest
ridge-like dorsal spine
E
dorsal process
anterodorsal spine
fenestra cochleae
stapedial muscle fossa
accessory ossicle
anteroventral spine
posterior process
F
dorsal process
anterodorsal spine
accessory ossicle
anteroventral spine
G
fenestra cochleae
anterodorsal spine
accessory ossicle
anteroventral spine
H
I
aperture for cochelar duct
aperture for endolymphatic duct
spiral cribriform tract
foramen singulare
proximal aperture for facial canal
dorsal process
ridge-like dorsal spine

individualized lateral tuberosity. On the ventral surface of the lateral tuberosity a conspicuous, semi-elliptical facet for the sigmoid process of the tympanic is observed. This facet is slightly concave anteroposteriorly and extends to the posterolateral margin of the mallear fossa. The mallear fossa is deep and relatively short anteroposteriorly (3 mm), facing posteroventromedially. Posteromedial to the mallear fossa is a small, relatively deep fossa (maximum diameter = 1 mm) that may correspond to the submallear fossa (*sensu* Tanaka & Fordyce 2017). This fossa is followed anteromedially by a short sulcus along the ventrolateral wall of the pars cochlearis. The distal opening of the facial canal reaches slightly more anterior than the fenestra vestibuli (= fenestra ovalis). The latter has an oval outline and is filled with part of the stapes. The moderately developed hiatus epitympanicus is 'V'-shaped in lateral view. It is defined posteriorly by a low ridge, directed laterally and slightly posteriorly. Posterior to this ridge, the surface of the bone is more irregular and pitted, whereas the surface of the hiatus is smooth. The area anterior to the posterior bullar facet is roughly flat, without any indication of a fossa incudis.

The narrow posterior bullar facet is directed posterolateroventrally. Its surface is slightly anteroposteriorly and mediolaterally concave, with the medial margin raising ventromedially as a thin plate. The lateral margin is distinctly less ventrally elevated, with the ventral surface possibly progressively turning lateral to laterodorsally (area somewhat damaged). The surface of the posterior bullar facet displays a few shallow ridges: one ridge is more conspicuous, at about one-third of the mediolateral width, and another ridge is close to the medial margin. The facial sulcus extends posteromedially, with its distal portion obscured by the anteromedial corner of the posterior bullar facet (facial crest). Also partly covered ventrally by the facial crest, the stapedial muscle fossa extends on the medial side of the posterior process, being poorly defined from about one-third of the length of the posterior bullar facet.

The posterior process as a whole differs markedly from that of all kogiids for which this bone is known, not being plate-like or posteriorly directed in lateral view (e.g. Kasuya 1973; Vélez-Juarbe *et al.* 2016). The dorsolateral side of this process is marked by a robust keel, directed anterodorsally towards the apex of the dorsal process (or superior process). The latter is moderately developed, less so than in *Aulophyseter morricei*, *Ferecetotherium kelloggi* (see Mchedlidze 1976), *Orycterocetus crocodilinus* and *Physeter macrocephalus*, reaching a level 10.4 mm dorsal to the ventral margin of the internal acoustic meatus. This dorsal process is not pointed in medial view, with a smoothly convex dorsal margin. It is more acute in anterior/posterior view, forming a ridge extending anteriorly as far as the dorsal spine just posterior to the depression on the mediodorsal surface of the anterior process. The dorsal spine is separated from the proximal opening of the facial canal by an oblique groove running posterolaterally from the anterior incisure along the internal acoustic meatus. The latter has a maximum transverse width of 7.4 mm (including the aperture for the facial canal) and an anteroposterior length of 5.0 mm. Its margins are not elevated. The proximal aperture for the facial canal has a maximum diameter of 2.0 mm and does not extend anteriorly beyond the anterior margin of the spiral cribriform tract. On the anterior corner of the aperture for the facial canal, a deep fissure connects the latter to the anterior incisure. The tiny foramen singulare is slit-shaped, with an anteroposteriorly directed long axis, located posteromedial to the aperture of the facial canal, at about the mid-length of the spiral cribriform tract, and separated from the aperture of the facial canal by a very low crest. The crest separating the foramen singulare from the spiral cribriform tract is slightly lower than the former crest. A low sulcus extends dorsally from the foramen singulare on the posterolateral wall of the internal acoustic meatus. The outline of the spiral cribriform tract is nearly circular, with a transverse width of 4.7 mm and an anteroposterior length of 4.7 mm. Located on the posterior wall of the pars cochlearis, the fenestra cochleae (= fenestra rotunda) has a mediolateral diameter of 3.5 mm and a dorsoventral diameter of 2.3 mm; a very short, narrow sulcus is located on its mediodorsal corner. The aperture for the cochlear duct is small (transverse diameter = 2.2 mm) and drop-shaped with an anterior point, 2.5 mm from the internal acoustic meatus and 1.4 mm from the aperture for the endolymphatic duct. The latter is anteroposteriorly compressed, with an anteroposterior diameter of 1.9 mm and a mediolateral diameter of about 3 mm (margins not sharply defined). This aperture is 1.5 mm from the internal acoustic meatus. The area around these two openings is relatively flat and smooth. The ventral surface of the pars cochlearis is slightly flattened, with a moderate bulge in the ventrolateral area. The ventral margin of the pars cochlearis along the stapedial muscle fossa (= crista interfenestralis) is regularly convex,

Figure 9. Right periotic of *Rhaphicetus valenciae* MUSM 2543 (holotype) in **A, B,** ventral, **C, D,** dorsal, **E,** medial, **F,** lateral, **G,** anterior, **H,** posterior, and **I**, anterodorsomedial views.

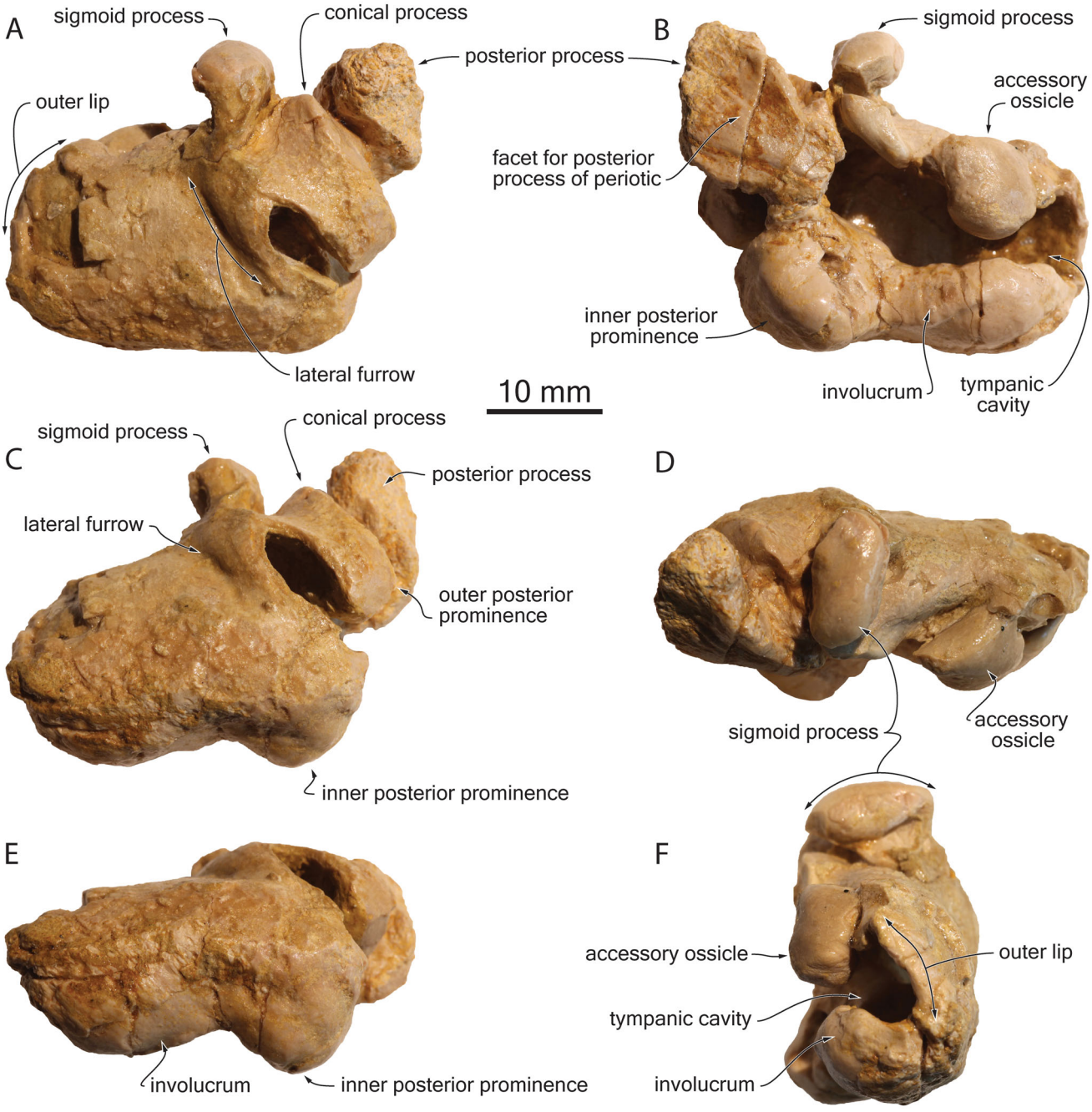

Figure 10. Left tympanic bulla of *Rhaphicetus valenciae* MUSM 2543 (holotype) in **A,** lateral), **B,** medial, **C,** ventrolateral, **D,** dorsal, **E,** ventral, and **F**, anterior views.

turning smoothly posterodorsally without any developed lateral caudal tympanic process (*sensu* Lambert *et al.* 2018).

Tympanic bulla. The left tympanic bulla is slightly damaged along the outer lip, with the accessory ossicle collapsed towards the tympanic cavity, small pieces of the sigmoid process missing, and an artificial opening on the dorsolateral wall, just anterior to the outer posterior prominence (Fig. 10). The posterior process is probably not complete posteromedially. By comparison with better preserved physeteroid ear bones and to facilitate the description, we consider the dorsal view to be the plane obtained when joining the base of the posterior

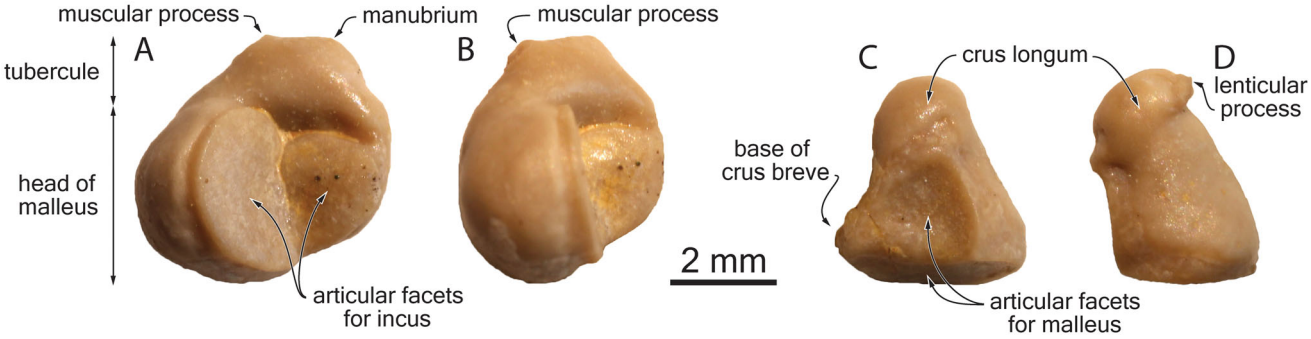

Figure 11. A, B, Left malleus and **C, D,** incus of *Rhaphicetus valenciae* MUSM 2543 (holotype).

process, the corner of the inner posterior prominence and the thickened anterior part of the involucrum.

In medial view, the involucrum displays the dorsal fold observed in all physeteroids (e.g. *Acrophyseter deinodon* and *Brygmophyseter shigensis*; see Kimura *et al.* 2006; Lambert *et al.* 2017). In dorsal view it is transversely thickened in its anterior region, with a slight narrowing at mid-length, and an abrupt thickening, both medial and lateral, towards the posterior part. The anterior portion of the involucrum does not turn medially as observed in *A. deinodon* and the isolated tympanoperiotic pair USNM 22953, tentatively referred to *Orycterocetus crocodilinus* (Kellogg 1965), being more similar instead to that of *B. shigensis* and *Zygophyseter varolai*. While projecting moderately far medially, as in *A. deinodon*, the inner posterior prominence remains medially shorter than in *Z. varolai* (see Bianucci & Landini 2006). In medial view, the dorsal margin rises abruptly from the anterior tip until a maximum height at the anteroposterior level of the accessory ossicle is reached; then this margin lowers slightly before rising steeply towards the posterior top of the involucrum, posterior to the level of the sigmoid process. In the anterior part of the involucrum, its dorsal margin is marked by a shallow, oblique ridge directed posteromedially. The ventral surface of the involucrum is slightly convex and rises posteromediodorsally (best seen in medial view).

The anterior margin of the tympanic is roughly transversely directed and straight, with no anterior spine, as in other known physeteroids. The ventral surface of the bone lacks any median furrow, being regularly transversely convex and slightly anteroposteriorly convex. The outer posterior prominence projects farther posteriorly than the inner prominence. Anterior to the prominences, the ventrolateral surface is excavated by a deep oblique groove (= lateral furrow of other odontocetes) running anterolaterally until the area just anterior to the sigmoid process. The area posterolateral to this groove is only partly preserved, but is prominent and more convex. Posterolateral to this prominent area, extending anterolaterally towards the base of the sigmoid process, a concave surface is observed between the sigmoid and conical processes. The latter is laterally pointed, extending posteromedially as an acute crest towards the tip of the outer posterior prominence. The conical process is clearly separated from the anterolateral margin of the posterior process: the tip of the former is 2.4 mm distant from the latter. The most medial part of the sigmoid process is directed anteromedially. A gradual posterolateral thickening is observed, with an abrupt lateral curve towards the main part of the process, being transversely directed, with a maximum anteroposterior thickness of 6.3 mm. This thickening is distinctly less pronounced than in the massive sigmoid process of *B. shingensis*. A deep groove is located at the base of the process on the anterior side.

The posterior wall of the tympanic is not well preserved (the middle part is missing), but it included a shallow interprominential notch. The latter appears to have been connected anterolaterally to the lateral furrow, described above on the ventrolateral surface, forming a continuous groove surrounding the outer posterior prominence. In addition to other physeteroids (e.g. *Kogia* spp. and *Physeter macrocephalus*; Kasuya 1973), a surprisingly similar condition is observed in the ziphiid-like Pliocene delphinoid *Australodelphis mirus* (Fordyce *et al.* 2002). The posterior process contacts the dorsal part of the outer posterior prominence, directed obliquely posterolaterally and turning ventrolaterally. The facet for the posterior process of the periotic is anteroposteriorly convex, with two main grooves, wide and shallow: one close to the medial margin and the other at about two-thirds of the width. The latter is laterally surrounded by an elevation of the lateral margin of the process, better marked at mid-length. Many additional narrow and shallow longitudinal grooves mark the facet. The posterior process is most likely incomplete posterolaterally, and its original length and maximum width cannot be estimated.

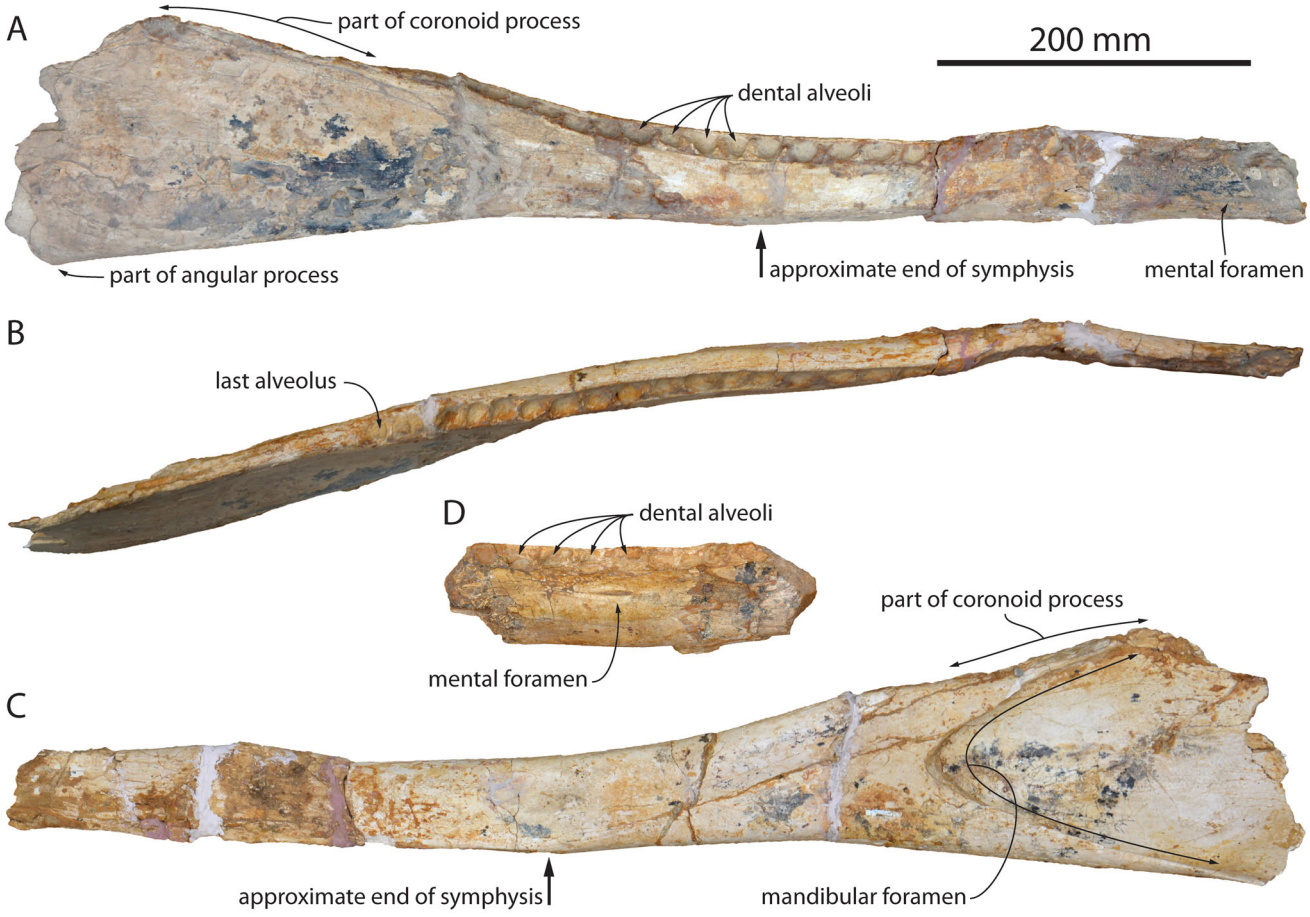

Figure 12. Mandible of *Rhaphicetus valenciae* MUSM 2543 (holotype). **A–C,** right mandible in **A,** lateral, **B,** dorsal, and **C,** medial views; **D,** fragment of the symphyseal region of the left mandible in lateral view.

Malleus. The left malleus of MUSM 2543 is complete, except for the anterior process, which is broken at its base and therefore totally missing (Fig. 11A, B). The head of the malleus, including the articulation facets for the incus, occupies a great portion of the posteromedial view, with only a short tubercule (about 1.3 mm), similar to the condition of several extant ziphiids and the heterodont odontocete *Inticetus vertizi*, but longer than in *Kogia* and *Physeter*, in which it is drastically reduced (Bianucci *et al.* 2010; Lambert *et al.* 2018). The muscular process is distinct on the corner of the tubercule above the largest articular facet for the incus. The manubrium is more difficult to detect, but it is probably located on the corner above the smallest articular facet, at the same height as the muscular process. The base of the anterior process is located high along the bone, in the tubercule region.

Incus. The left incus articulates perfectly with the corresponding malleus. Its crus breve is broken at its base and the lenticular process is slightly damaged (Fig. 11C, D). Compared to the smaller articular facet for the malleus, the crus longum is relatively short (shorter than in *Acrophyseter deinodon* and *Physeter*, more similar to *Kogia*). The base of the crus breve is close to the largest articular facet for the malleus, closer than in, for example, *Zygorhiza*, *Platanista* and ziphiids (see Lambert *et al.* 2017).

Mandibles (Fig. 12)

Preserved parts include an 830 mm long portion of the right mandible, lacking the anterior tip, the condyle, and part of the coronoid and angular processes; and a smaller, 230 mm long fragment of the left mandible, posterior to the mandibular symphysis. The mandible is proportionally long, with a moderately robust mandibular symphysis. At the posterior end of the symphysis, the joined dentaries were nearly as high as wide. The symphysis is unfused and long, ending 360 mm posterior to the incomplete anterior tip of the mandible and about 240 mm anterior to the anterior margin of the

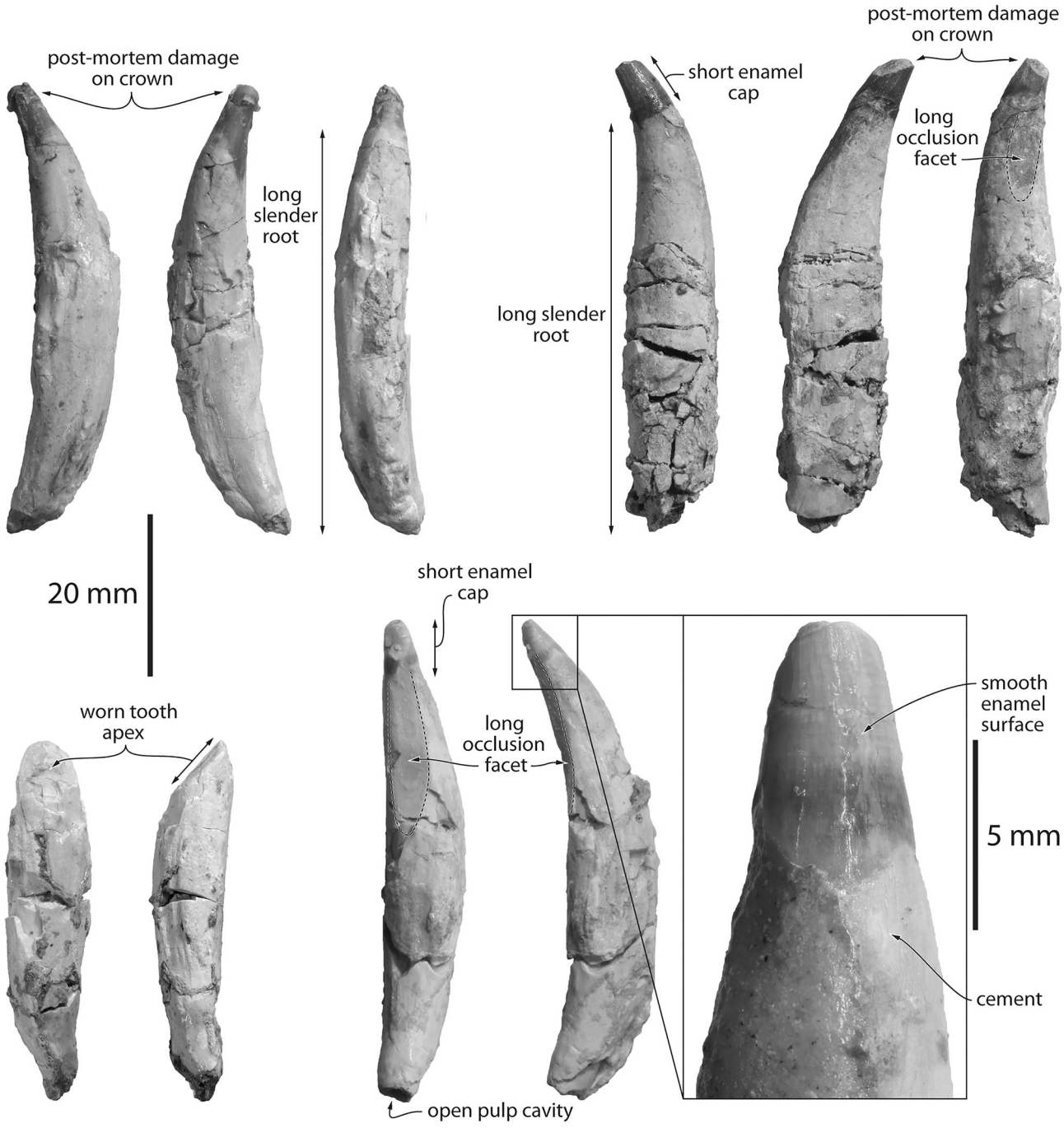

Figure 13. Four detached teeth of *Rhaphicetus valenciae* MUSM 2543 (holotype).

mandibular foramen. The surface of the symphysis is excavated by pits and grooves. The ventral margin of the mandible is straight in lateral view under the large mandibular foramen. A slight concavity marks the area between this foramen and the posterior end of the symphysis, where this ventral margin becomes slightly convex, before gradually raising anterodorsally. As a whole the mandible is significantly less curved in lateral view compared to that of *Idiorophus patagonicus*, *Physeterula dubusi*, *Zygophyseter varolai* and, to an even greater extent, *Acrophyseter* spp. The mandibular foramen is large, roughly occupying the whole posterior height of the mandible, with a regularly rounded anterior margin differing from the more pointed anterior

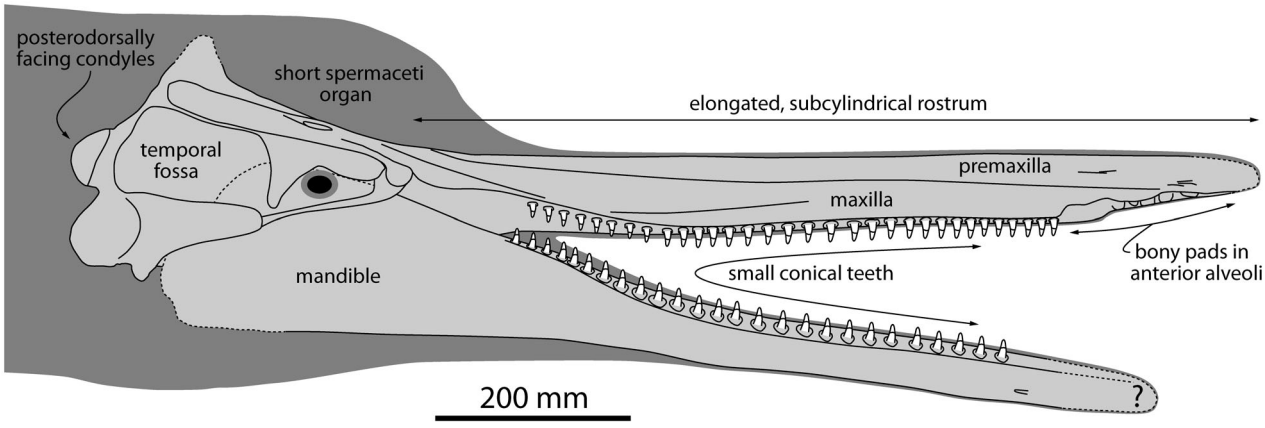

Figure 14. Reconstruction of the skull of *Rhaphicetus valenciae* MUSM 2543 (holotype) in right lateral view. Stippled lines for main reconstructed bony parts; dark grey shading for a hypothetical reconstruction of the soft tissue outline of the head, including an anteriorly short spermaceti organ. The anterior tip of the mandibles being missing, the anterior extent of the lower jaw remains unknown.

margin seen in *Acrophyseter deinodon*, *Z. varolai* and young individuals of *Physeter macrocephalus*. Only a couple of mental foramina can be observed, one in the anterior portion of the right mandible and the other at mid-length of the fragment of left mandible, 14 mm below the lateral edge of the alveolar row.

Twenty-six small alveoli for single-rooted teeth are counted on the preserved portion of the right alveolar row, 12 to 13 of them posterior to the symphysis (Fig. 12A, B). This number of post-symphysis alveoli is higher than in *Acrophyseter* spp., *Kogia* spp., *P. macrocephalus*, *P. dubusi* and *Z. varolai*, probably closer to that of *Idiorophus patagonicus*. Starting posteriorly with a transverse diameter of about 12 mm, alveoli increase in size anteriorly, reaching a maximum diameter of 15 mm at the posterior end of the symphysis. Although not fully freed from the indurated sediment, it can be seen that alveoli are more than 12 mm deep. Interalveolar septa are short, ranging from 3 mm between posterior-most alveoli to 8 mm at the posterior end of the symphysis. Whereas the posterior alveoli face dorsally, the alveolar row gradually shifts anteriorly to a more dorsolateral orientation; at the end of the symphysis, the lateral edge of the alveolar row is markedly lower than the medial edge, such that the surface joining these two lines forms an angle of about 45° with the horizontal plane. Missing its posterodorsal part, the dorsal margin of the coronoid process is rectilinear and only rises gradually posterodorsally, much less than in *A. deinodon*.

Detached teeth (Fig. 13)

The few preserved teeth are proportionally small, and slender as in *Aulophyseter morricei*, *Idiorophus patagonicus*, *Kogia* spp. and *Orycterocetus crocodilinus*, with a short crown; the total tooth length reaches 56 and 59 mm in the best-preserved teeth; the maximum diameter of the root does not exceed 13–14 mm and the maxiumum crown length is 10 mm, with a maximum crown diameter of 6 mm. The ratio between the maximum root diameter and bizygomatic width of the skull is 0.027, considerably smaller than in macroraptorial stem physeteroids (see Lambert *et al.* 2017). A very thin cap of enamel (less than 0.25 mm) covers the simple, conical crown with no carina, a condition similar to that of *I. patagonicus* (see Lydekker 1893), but differing from that of several other physeteroids (e.g. *A. morricei*, *Kogia* spp., *O. crocodilinus*, *Physeter macrocephalus* and *Physeterula dubusi*), which lack enamel on teeth. The enamel surface is smooth, lacking any ornamentation, thus differing from a series of stem physeteroids displaying a strong ornamentation on a thicker enamel layer (e.g. Hampe 2006; Lambert & Bianucci 2019). An elongated occlusion facet, extending along the root's surface, is observed in several teeth (as, for instance, in *O. crocodilinus*; Kellogg 1965), with a maximum length of 19 mm. Parts of the teeth display an obliquely truncated crown apex, but in at least some of these teeth this is a result of post-mortem damage. One tooth (Fig. 13) lacks the whole crown region and part of the root, displaying an oblique, flat wear surface. A similar oblique wear surface is regularly observed on lower teeth located posterior to the mandibular symphysis in *Physeter macrocephalus*, with the wear surface facing dorsomedially (e.g. MNHN A3245); it has also been noted in one tooth of the kogiid *Pliokogia apenninica* (Collareta *et al.* 2019) and in the bizarre prognathous Pliocene phocoenid *Semirostrum ceruttii* (Racicot *et al.* 2014).

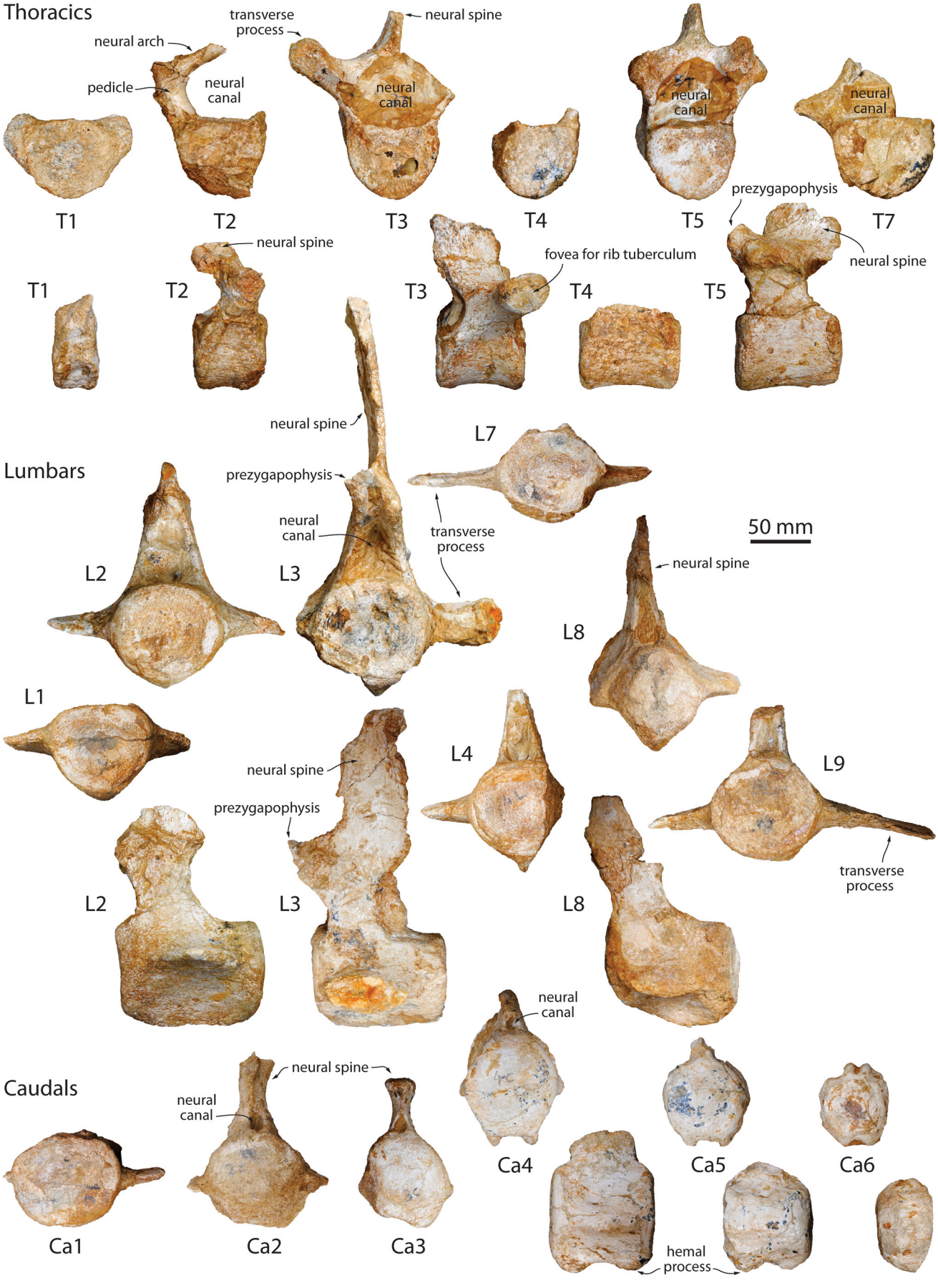
Thoracics
transverse process
neural spine
neural arch
pedicle
neural canal
neural canal
neural canal
neural canal
prezygapophysis
T1
T2
T3
T4
T5
T7
neural spine
fovea for rib tuberculum
neural spine
T1
T2
T3
T4
T5
neural spine
L7
Lumbars
prezygapophysis
neural canal
transverse process
50 mm
neural spine
L2
L3
L8
L1
neural spine
L4
L9
prezygapophysis
transverse process
L2
L3
L8
neural canal
neural spine
Caudals
neural canal
Ca4
Ca5
Ca6
Ca1
Ca2
Ca3
hemal process

Unfortunately, none of the detached teeth of MUSM 2543 could be relocated along the tooth rows, and the potential causes of such intense wear remain highly speculative. If posteriorly located, this tooth may have been abraded by repetitive rubbing of the tongue and/or prey items when swallowing (via suction?), producing wear that could have been accentuated by the presence of abrasive sediment. As mentioned above, the pulp cavity is not completely filled in the preserved teeth; its maximum diameter reaches 35 mm.

Vertebrae (Fig. 15)

A series of 22 vertebrae were found associated with the cranium: seven thoracics, nine lumbars and six caudals (Table 2). Most of those are not complete, sometimes even missing portions of the centrum, and only a few retain the neural arch and parts of the transverse processes. Only limited anatomical information is thus available, and the position of each vertebra along the vertebral column is estimated relative to the changes in the dimension of the centrum; numbers provided for each vertebra correspond only to relative, not exact positions. The vertebral count as preserved is considerably lower than in *Physeter macrocephalus* and *Kogia* spp. for the thoracics and caudals (see Flower 1867a; Van Beneden & Gervais 1880; Yamada 1954; Omura *et al.* 1962; Ross 1984; Rice 1989), thus not providing any meaningful assessment of the minimum number of vertebrae per region of the column in MUSM 2543. A minimum of nine lumbars is close to the counts in *Brygmophyseter shigensis* (10; Kimura *et al.* 2006), *Kogia* spp. (10–12) and *Zygophyseter varolai* (10; Bianucci & Landini 2006), and slightly higher than in *P. macrocephalus* (eight).

Posterior thoracics (from T4) display a centrum that is longer than wide or high, a significant difference with *B. shigensis* and *P. macrocephalus* (see Flower 1867a; Buchholtz 2001; Kimura *et al.* 2006). In addition, the base of neural spines (e.g. in T3 and T5) is anteroposteriorly longer than in the latter, more similar to *Kogia* spp.

In all preserved lumbars the centrum is longer than wide or high, a condition that, again, differs from that of *P. macrocephalus*. Proportions of vertebrae in this part of the vertebral column were closer to those of *Delphinapterus leucas* and *Ziphius cavirostris*, for example, corresponding to pattern 2 of Buchholtz (2001), which predicts an enhanced torso flexibility compared to *P. macrocephalus*. Lumbars of *Z. varolai* are also elongated (Bianucci & Landini 2006). Preserved lumbars lack the highly unusual bifurcated ventral projection observed along the sagittal plane of the centrum in *Kogia* spp. and, to a lesser extent *P. macrocephalus* (Van Beneden & Gervais 1880; Yamada 1954). The neural spine is dorsoventrally high and roughly vertical in L3, a feature that is not observed in lumbars of *Kogia* spp. and *P. macrocephalus*, the neural spine being tilted posterodorsally in these taxa.

Except for the posteriormost Ca6, preserved caudals have a centrum that is longer than high or wide, as in *Z. cavirostris* (Buchholtz 2001). The centrum of the preserved posterior caudals (Ca4–6) is higher than wide, corresponding to the laterally compressed caudal tail stock (*sensu* Buchholtz 2001), just anterior to the dorsoventrally flattened vertebrae of the fluke region (not preserved here). In *P. macrocephalus* centra are higher than wide in caudals 8–12 (Omura *et al.* 1962), whereas in *B. shigensis* this condition occurs in caudals 5–9.

Sternum (Fig. 16A)

The manubrium (first sternal element) of MUSM 2543 is partly preserved, but it is broken in several pieces and only a few original margins are retained. One large prominence in one corner of the main fragment may correspond to the anterolateral part of the bone. A large dorsoventral opening, with a maximum diameter of 35 mm, does not seem to be centred. Differing from *Kogia* spp., in which the anterior margin of the manubrium is cut by a deep notch (Schulte & Smith 1918; Yamada 1954), in the extant *Physeter macrocephalus* this bone is similarly pierced by a large sagittal opening (e.g. Flower 1867a; Van Beneden & Gervais 1880; Omura *et al.* 1962). However, in the latter the left and right parts of the bone remain at least partly unfused in adults, differing from the condition seen in MUSM 2543.

Figure 15. Thoracic, lumbar and caudal vertebrae of *Rhaphicetus valenciae* MUSM 2543 (holotype). Numbers correspond to relative positions along the vertebral column, not exact positions. T1 in anterior/posterior and lateral views; T2 in anterior and right lateral view; T3 in anterior and right lateral views; T4 in anterior/posterior and lateral views; T5 in anterior and left lateral views; T7 in posterior view; L1 in anterior/posterior view; L2 in posterior and left lateral views; L3 in anterior and left lateral views; L4 in posterior view; L8 in left lateral and anterior views; L9 in anterior view; Ca1 in anterior/posterior view; Ca2 in posterior view; Ca3 in anterior view; Ca4 in anterior/posterior and lateral views; Ca5 in anterior/posterior and lateral views; and Ca6 in anterior/posterior and lateral views.

Table 2. Vertebral measurements (in mm) of *Rhaphicetus valenciae* gen. et sp. nov. MUSM 2543 (holotype). **Abbreviations: +**, incomplete; -, missing data; **ant.**, anterior; **Ca**, caudal; **e**, estimate; **L**, lumbar; **post.**, posterior **T**, thoracic; **transv.**, transverse. Numbers do not correspond to exact positions but to relative positions along the vertebral column.

	Centrum length	Centrum ant. width	Centrum ant. height	Centrum post. width	Centrum post. height	Neural canal ant. width	Width across transv. processes
T1	35	78	62	74	63	–	–
T2	58	68	58	68	60	–	–
T3	63	70	56	70	56	68	e166
T4	78	64	55	64	58	–	–
T5	80	69	58	74	+55	60	e110
T6	90	–	–	–	–	–	–
T7	–	–	–	77	62	–	–
L1	97	e80	–	77	68	–	–
L2	105	e82	73	85	74	42	–
L3	113	80	e76	–	–	39	–
L4	119	–	–	e86	80	34	–
L5	120	74	80	–	–	34	–
L6	120	76	78	e78	e77	22	–
L7	115	90	78	92	–	–	–
L8	110	–	–	93	e82	19	–
L9	107	91	88	–	–	20	e300
Ca1	103	90	+77	–	–	–	–
Ca2	+87	–	–	–	–	11	–
Ca3	96	–	–	e80	+82	e12	–
Ca4	88	76	79	71	80	8	–
Ca5	74	70	72	63	68	–	–
Ca6	+48	–	–	55	57	–	–

Ribs (Fig. 16B)

Only a few rib fragments are preserved, lacking capitula and tubercula, and ranging from transversely broader, anteroposteriorly flattened anterior ribs to more slender posterior ribs with a more rounded cross-section. None of the rib fragments displays evidence of pachyostosis.

Body length estimates

With a bizygomatic width (BZW) of 505 mm and an estimated condylobasal length (CBL) of 1308 mm, we calculated the body length (BL) of *Rhaphicetus valenciae* MUSM 2543 following the three equations proposed by Lambert *et al.* (2010). The equation based on measurements of *Physeter macrocephalus* [BL = (4.23 × BZW + 222.04) + CBL, in cm] results in an estimate of 5.66 m. The first equation based on measurements of *Zygophyseter varolai* (BL = 6.738 × BZW + CBL) results in an estimate of 4.71 m. The second equation based on measurements of *Zygophyseter varolai* (BL = 7.41 × BZW + CBL) results in an estimate of 5.05 m. Note that in all estimates calculated here the condylobasal length is added to the estimate for postcranial length, thus allowing us to take into account the considerably elongated rostrum in MUSM 2543. Equations that do not include the condylobasal length (e.g. Pyenson & Sponberg 2011) may therefore result in an underestimated value for longirostrine taxa (BL = 4.59 m with the Pyenson & Sponberg equation for stem physeteroids). The body length of MUSM 2543 most likely ranged between 4.7 and 5.7 m, close for example to the extant beaked whale *Mesoplodon bidens*, and, among physeteroids, intermediate between the smaller *Acrophyseter deinodon* (4.0–4.3 m; Lambert *et al.* 2017) and the larger *Zygophyseter varolai* (6.5–7.0 m; Bianucci & Landini 2006), and closer to *Diaphorocetus poucheti* (Paolucci *et al.* 2020).

Phylogenetic analysis

The first heuristic searches, with both equal weighting and down-weighting of homoplastic characters, produced a surprising sister-group relationship between the macroraptorial giant stem physeteroid *Livyatan melvillei* and the family Kogiidae. We thus removed the highly homoplastic character 1, related to rostrum length, from subsequent analyses. The heuristic search with equal weightings resulted in 648 most parsimonious trees, with tree length = 143, consistency index (CI) = 0.53 and retention index (RI) = 0.73. The strict consensus tree is shown in Figure 17. It should be noted that most bootstrap support values remain relatively low, probably due to the limited number of morphological characters

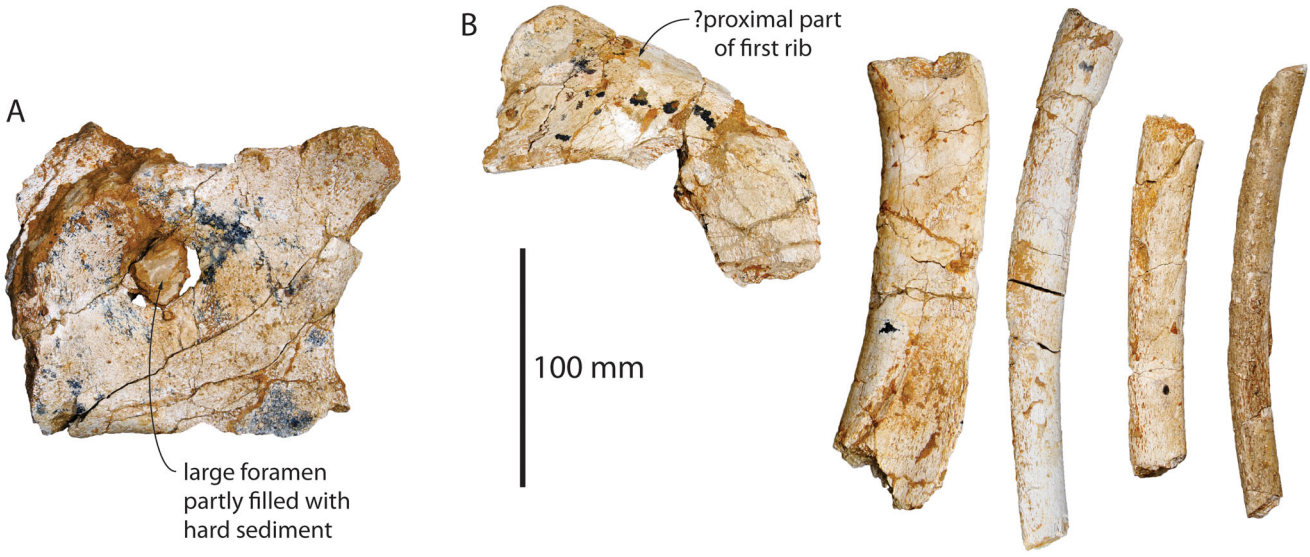

Figure 16. Sternum and ribs of *Rhaphicetus valenciae* MUSM 2543 (holotype). **A,** partial first segment (manubrium) of the sternum in dorsal view; **B,** rib fragments. Because parts of the margins of the manubrium are not preserved and due to its apparent asymmetry, the orientation of this bone remains unresolved.

available and the fragmentary state of the type material for some of the species analysed here. Phylogenetic relationships discussed here should thus be treated with caution. *Rhaphicetus valenciae* is recovered as one of the earliest stem physeteroids, branching just after *Eudelphis mortezelensis*. Differing from previous analyses (e.g. Velez Juarbe *et al.* 2015; Lambert *et al.* 2017; Collareta *et al.* 2019; Benites-Palomino *et al.* 2020; Paolucci *et al.* 2020), *Acrophyseter* spp. branch before other macroraptorial stem physeteroids, followed by *Zygophyseter varolai*, whereas relationships of *Brygmophyseter shigensis* and *Livyatan melvillei* with crown Physeteroidea (Kogiidae + Physeteridae) remain unresolved. Also contrasting with previous analyses (Lambert *et al.* 2017; Collareta *et al.* 2019), '*Aulophyseter*' *rionegrensis* is recovered as a physeterid, instead of a late-diverging stem physeteroid. *Placoziphius duboisi* is here found as sister group to *Diaphorocetus poucheti*, in a clade also including '*A.*' *rionegrensis* and *Orycterocetus crocodilinus*, whereas in previous analyses it was recovered as more closely related to *Physeter macrocephalus* and fossil relatives (Lambert *et al.* 2017; Collareta *et al.* 2019), or outside crown Physeteroidea (Benites-Palomino *et al.* 2020; Paolucci *et al.* 2020). Compared to Collareta *et al.* (2019) and Benites-Palomino *et al.* (2020), relationships within Kogiidae are less well resolved, but not contradictory (but see Alfsen *et al.* in press for a reassessment of the status of the genus *Thalassocetus*, not included in the present analysis).

The analysis with down-weighting of homoplastic characters (k = 3) produces a strict consensus tree with several unexpected results (see Supplementary material, Fig. S1), including (1) a sister-group relationship between *E. mortezelensis* and macroraptorial stem physeteroids, except *L. melvillei*; (2) *L. melvillei* being resolved as sister group to the normally recognized Kogiidae; (3) a less inclusive Physeteridae, including only *Aulophyseter morricei*, *Idiophyseter merriami* and *P. macrocephalus*; and (4) several taxa (*I. patagonicus*, *Physeterula dubusi* and *Orycterocetus crocodilinus*) also recovered as stem taxa to the normally recognized Kogiidae. Our first analysis (with equal weighting) is thus considered much more convincing, and, although displaying relatively low bootstrap values, better reflects our current understanding of physeteroid phylogenetic relationships.

Discussion

Comparison with other physeteroids and phylogenetic relationships

As presented in the species diagnosis, morphological characters from the facial region (presence of a supracranial basin and extreme asymmetry of the bony nares) and ear bones (periotic, tympanic and malleus) unambiguously refer *Rhaphicetus valenciae* gen. et. sp. nov. to the superfamily Physeteroidea. Dated from the early Burdigalian (19.0 to 18.02 Ma), the new species is thus

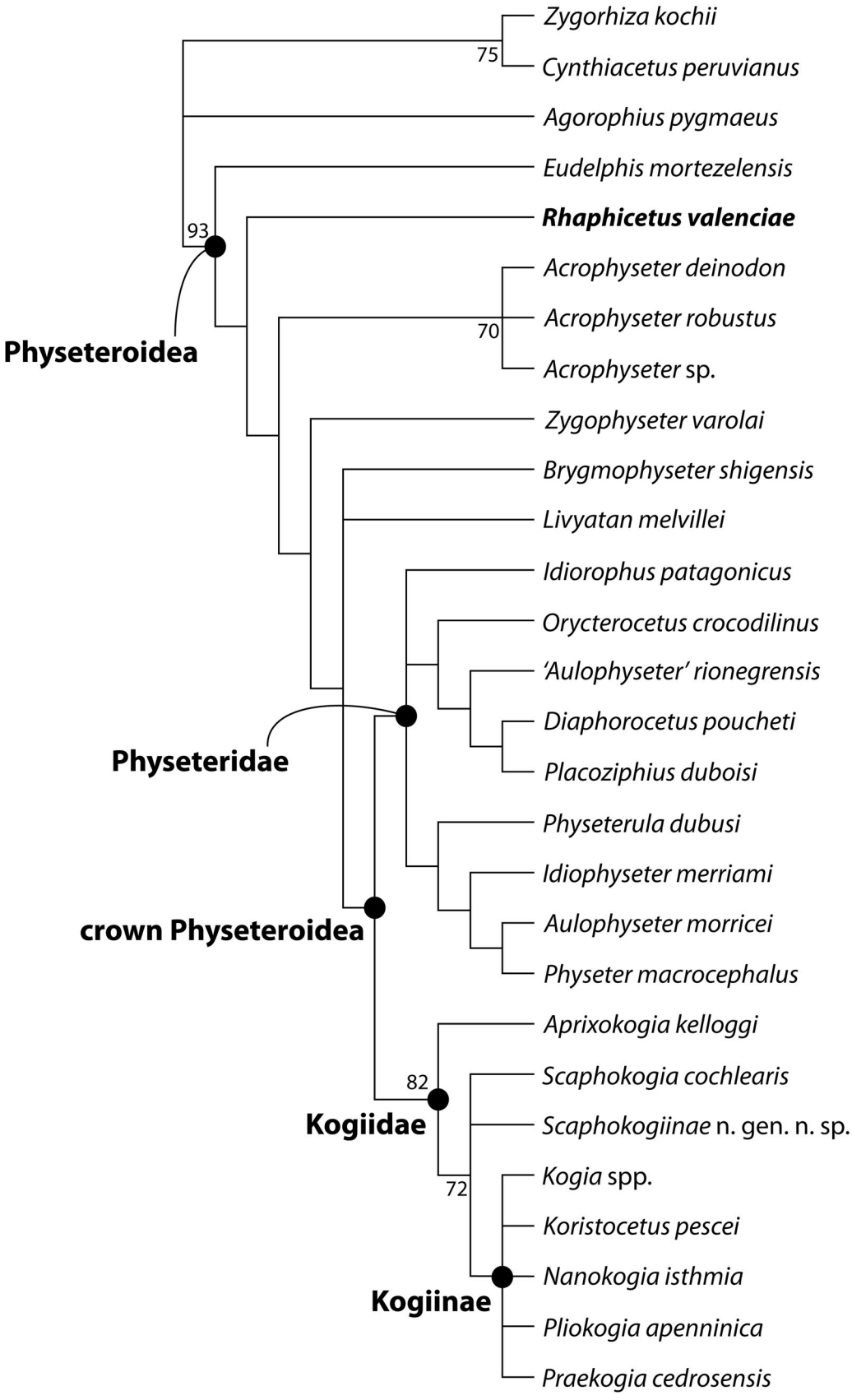
Zygorhiza kochii
75
Cynthiacetus peruvianus
Agorophius pygmaeus
Eudelphis mortezelensis
Rhaphicetus valenciae
93
Acrophyseter deinodon
Acrophyseter robustus
70
Acrophyseter sp.
Physeteroidea
Zygophyseter varolai
Brygmophyseter shigensis
Livyatan melvillei
Idiorophus patagonicus
Orycterocetus crocodilinus
'Aulophyseter' rionegrensis
Diaphorocetus poucheti
Physeteridae
Placoziphius duboisi
Physeterula dubusi
Idiophyseter merriami
crown Physeteroidea
Aulophyseter morricei
Physeter macrocephalus
Aprixokogia kelloggi
82
Scaphokogia cochlearis
Kogiidae
Scaphokogiinae n. gen. n. sp.
72
Kogia spp.
Koristocetus pescei
Nanokogia isthmia
Kogiinae
Pliokogia apenninica
Praekogia cedrosensis

one of the geologically oldest members of the clade. Indeed, except for *Ferecetotherium kelloggi*, a poorly known physeteroid from the Caucasus for which the stratigraphic context still needs clarification (Mchedlidze 1976; Marx *et al.* 2016), the oldest stratigraphically well-constrained physeteroid records date from the early Miocene, with *Placoziphius duboisi* from the late Aquitanian to early Burdigalian of Belgium (Lambert 2008) and *Diaphorocetus poucheti* and *Idiorophus patagonicus* from the early Burdigalian of Argentina (Paolucci *et al.* 2020). In addition to being one of the earliest sperm whales (the oldest for the whole Pacific Ocean), and although relationships in our favoured phylogenetic tree remain poorly supported, the medium-sized *R. valenciae* (body length estimated to be between 4.7 and 5.7 m) is recovered as one of the earliest stem physeteroid lineages, branching before the modern families Kogiidae and Physeteridae. It therefore potentially provides clues to the ancestral morphotype for sperm whales. Nevertheless, the new taxon is also characterized by a series of autapomorphic features, including the posterior position of the main dorsal infraorbital foramina, the elongated rostrum (nearly 75% of the condylobasal length), the high upper tooth count (at least 36 teeth per row), and the unique filling of anterior upper dental alveoli by bony pads (discussed below in the section on dental reduction). More specific anatomical differences with physeteroid subgroups (macroraptorial sperm whales, Kogiidae and Physeteridae) are also discussed below (Palaeobiology section), in relation to feeding strategies.

Unique pattern of dental reduction

A decrease in tooth count is a commonly observed feature among odontocetes, occurring convergently in several lineages, for example among delphinids, kogiids, physeterids, monodontids, xenorophids and ziphiids (Werth 2006; Bianucci *et al.* 2016; Boessenecker *et al.* 2017; Lambert *et al.* 2017). In all these lineages, if a series of functional teeth are retained, the reduction of the tooth count is associated with a shortening of the alveolar row, with the last alveolus located more anteriorly in more derived species. From a developmental viewpoint, ontogenetic tooth loss has been described in the delphinid *Peponocephala electra*, with bony tissue inside the alveoli pushing out the teeth (Kurihara *et al.* 2016); here again, this process starts in the posterior-most teeth.

In *Rhaphicetus valenciae* MUSM 2543, interpreted here as representing a relatively aged individual, the filling of alveoli is limited to the anterior-most portion of the rostrum (apical and subapical teeth), a feature that is highly unusual among cetaceans. In addition to several tusk-bearing ziphiids retaining a full set of upper and lower teeth, but displaying some degree of dental reduction just posterior to the mandibular tusks (Mead & Payne 1975; Muizon 1984), we only found two other examples of odontocetes bearing a full set of functional teeth in the posterior part of the tooth row and displaying some degree of anterior tooth loss. The first example is among members of the Miocene family Eurhinodelphinidae, which are characterized by an elongated premaxillary part of the rostrum that is edentulous (e.g. Abel 1901; Lambert 2005b). The second example is the highly unusual phocoenid *Semirostrum ceruttii*, having an edentulous, elongated symphyseal part of the mandible (Racicot *et al.* 2014). Interestingly, in both examples the edentulous region is significantly anteriorly longer than the opposite jaw: the mandible is markedly shorter in eurhinodelphinids (Kellogg 1925; Lambert 2005c), whereas the rostrum is shorter in *S. ceruttii* (Racicot *et al.* 2014). Such a difference in the extent of the jaw bearing the edentulous portion may suggest that the rostrum of *R. valenciae* was somewhat longer than the mandible (Fig. 14). Unfortunately, the mandible of MUSM 2543 is incomplete anteriorly, and until a more complete specimen is found we will not be able to test this hypothesis.

Interestingly, in the case of *Physeter macrocephalus* the reduction of the functional upper dentition occurs with the retention of teeth; maxillary teeth still grow, but they generally do not erupt (e.g. Boschma 1938). Such a process differs markedly from the filling of dental alveolae observed in *Rhaphicetus valenciae*, providing an additional clue to the convergent evolution of dental reduction in several physeteroid lineages.

Palaeobiology

Rhaphicetus valenciae contrasts with Miocene physeteroids that have been interpreted as macroraptorial feeders (e.g. *Acrophyseter* spp., *Albicetus oxymycterus*, *Brygmophyseter shigensis*; *Livyatan melvillei* and *Zygophyseter varolai*; Bianucci & Landini 2006; Lambert *et al.* 2014, 2017; Lambert & Bianucci 2019) in the proportionally small, more slender teeth, the

Figure 17. Phylogenetic relationships of *Rhaphicetus valenciae* among stem physeteroids. Consensus of 648 most parsimonious trees resulting from the equal-weighting heuristic search. Tree length 143; consistency index (CI) 0.53; retention index (RI) 0.73. Bootstrap values higher than 50 are indicated at nodes.

enamel layer on teeth being much thinner, with no ornamentation, and the proportionally dorsoventrally lower temporal fossa (Fig. 14). On the other hand, it differs from the highly specialized, suction-feeding, and predominantly teuthophagous extant physeteroids *Kogia* spp. and *Physeter macrocephalus* (Rice 1989; Werth 2004, 2006; Bloodworth & Marshall 2005; Staudinger *et al.* 2014) in the retention of functional upper teeth, the presence of enamel on teeth, the anteroposteriorly longer temporal fossa and the supracranial basin not significantly invading the dorsal surface of the rostrum. It further differs markedly from *Kogia* spp. in the much longer rostrum.

With its elongated rostrum, *R. valenciae* has an estimated rostral index of 0.73, in the upper part of the range of longirostrine taxa (McCurry & Pyenson 2018) and greater than in most extant odontocetes. The rostrum's cross-section was approximately circular, thus not implying any favoured direction for movement (see McCurry & Pyenson 2018). Combined with the long snout and the retention of a long temporal fossa, the relatively high number (compared to other physeteroids) of slender, pointed upper and lower teeth suggests that teeth were used to grasp relatively small prey, possibly via rapid movements of the head (= snapping), as for example in the Amazon dolphin *Inia geoffrensis* and, presumably, a series of extinct hyper-longirostrine odontocetes (Hocking *et al.* 2017; McCurry & Pyenson 2018). Proportions and degree of fusion of the cervical vertebrae, unknown in the holotype, could provide further indications of the prey capture behaviour of *R. valenciae*. The orientation of the occipital condyles, facing posterodorsally and contrasting with, for example, *Inia geoffrensis*, *Kogia* spp. and *Pontoporia blainvillei*, suggests that the position of the head in resting position, with the rostrum pointing upwards compared to the rest of the body, was different from that in the extant *Kogia* spp. and *P. macrocephalus*, characterized by the rostrum pointing downwards.

As proposed for other odontocetes characterized by an edentulous anterior part of the rostrum or mandible (eurhinodelphinids and *Semirostrum ceruttii*), the loss of a series of teeth at the apex of the rostrum (a condition that, at first sight, may appear counterintuitive, as *R. valenciae* displays one of the highest tooth counts among physeteroids) may correspond to the use of the latter as a probing tool, for example, in soft sediment (Lambert 2005c; Racicot *et al.* 2014). The truncated ventral margin of the edentulous part of the rostrum, producing a tapering outline in lateral view, would especially match such a prey detection strategy, together with the series of sulci detected on the lateral surface of the premaxilla in that region, suggesting some degree of vascularization/innervation of the rostrum tip. Such a benthic feeding behaviour would also explain the extent of apical wear observed on one of the teeth of MUSM 2543 (Fitzgerald 2010; Racicot *et al.* 2014). Still, more data are needed regarding the position of worn teeth along the jaws, the morphology of the apex of the mandible (which may have been shorter than the rostrum), and digestive tract contents (see Lambert *et al.* 2015 for an ecological interpretation of another extinct longirostrine odontocete, with a robust rostrum, from the Peruvian Miocene) to further test this hypothesis. Alternatively, a longer upper jaw could have been used to strike and stun fish higher in the water column, in a way similar to istiophorid and xiphiid osteichthyans (billfish; Habegger *et al.* 2015).

Conclusions

The description and comparison of a finely preserved physeteroid partial skeleton (including one of the most complete skulls for an extinct sperm whale) from the lower Miocene (19–18 Ma) of the Chilcatay Formation (southern coast of Peru) leads to the definition of a new genus and species, *Rhaphicetus valenciae*. This medium-sized sperm whale is recovered as an early diverging stem physeteroid in our phylogenetic analyses. However, such a basal position contrasts with a series of probably autapomorphic features observed in *R. valenicae*, including the extremely elongated snout, high tooth count, and unique pattern of dental reduction at the apex of the rostrum (through the filling of upper alveoli by bony pads). All these morphological characters strongly support the interpretation of the feeding strategy of this new taxon as differing markedly from both the macroraptorial stem physeteroids and the suction-feeding extant sperm whales *Kogia* spp. and *Physeter macrocephalus*. Whereas the edentulous apex of the upper jaw may have been used to contact/stun fast-swimming prey or to probe in soft sediment, the long, cylindrical rostrum bearing numerous, proportionally small teeth most likely allowed it to grasp, by snapping, relatively small prey items, gradually transporting them to the back of the mouth before swallowing them roughly intact.

The discovery and study of similarly well-preserved specimens from other early diverging, late Oligocene to early Miocene stem physeteroids would shed further light on the first steps of the evolutionary history of the superfamily and its phylogenetic relationships with extinct non-physeteroid odontocetes, thus potentially providing new clues for the ecological characterization

of the very first members of this surprisingly highly disparate and long-living cetacean clade.

Acknowledgements

We wish to warmly thank W. Aguirre, G. Bosio, C. Di Celma and E. Malinverno for their help during fieldwork; W. Aguirre for his help during the excavation of MUSM 2543 and for its preparation at MUSM; and R. E. Fordyce, an anonymous reviewer, and the editor A. Lister for their constructive comments. We also thank the following for facilitating access to the collections of modern and fossil cetaceans under their care: R. Salas-Gismondi and R. Varas-Malca (MUSM); D. J. Bohaska, J. G. Mead, C. Potter and N. D. Pyenson (USNM); S. Bruaux, G. Lenglet and O. Pauwels (IRSNB); L. G. Barnes and V. R. Rhue (LACM); R. E. Fordyce (OU), C. Lefèvre (MNHN), A. G. Rol (ZMA), H. van Grouw (NNML), S. Farina and C. Sorbini (MSNUP); the late A. Varola (MAUS); and Z. Gasparini and L. H. Pomi (MLP).

This research was supported by funding from the University of Pisa (PRA_2017_0032) to GB, a grant from the Italian Ministero dell'Istruzione, dell'Università e della Ricerca (MIUR) (PRIN Project, 2012YJSBMK EAR- 9317031) to GB, and a National Geographic Society Committee for Research Exploration grant (GEFNE 177-16) to OL.

Supplemental material

The supplemental material includes material for the phylogenetic analysis (list of characters, character-taxon matrix, and consensus tree resulting from the analysis with down-weighting of homoplastic characters). Supplementary material for this article can be accessed here: https://doi.org/10.1080/14772019.2020.1805520.

ORCID

Olivier Lambert http://orcid.org/0000-0003-0740-5791
Christian de Muizon http://orcid.org/0000-0002-1247-8867
Mario Urbina http://orcid.org/0000-0002-1898-9051
Giovanni Bianucci http://orcid.org/0000-0001-7105-0863

References

Abel, O. 1901. Les dauphins longirostres du Boldérien (Miocène supérieur) des environs d'Anvers. I. *Mémoires du Musée Royal d'Histoire Naturelle de Belgique*, **1**, 1–95.

Alfsen, A., **Bosselaers, M.** & **Lambert, O.** (In press). New sperm whale remains from the late Miocene of the North Sea and a revised family attribution for the small crown physeteroid *Thalassocetus*. *Comptes Rendus Palevol*. doi:10.1016/j.crpv.2008.06.002

Benites-Palomino, A., **Vélez-Juarbe, J.**, **Salas-Gismondi, R.** & **Urbina, M.** 2020. *Scaphokogia totajpe*, sp. nov., a new bulky-faced pygmy sperm whale (Kogiidae) from the late Miocene of Peru. *Journal of Vertebrate Paleontology*, **39**, e1728538. doi:10.1080/02724634.2019.1728538

Bianucci, G., & **Landini, W.** 2006. Killer sperm whale: a new basal physeteroid (Mammalia, Cetacea) from the late Miocene of Italy. *Zoological Journal of the Linnean Society*, **148**, 103–131. doi:10.1111/j.1096-3642.2006.00228.x

Bianucci, G., **Lambert, O.** & **Post, K.** 2010. High concentration of long-snouted beaked whales (genus *Messapicetus*) from the Miocene of Peru. *Palaeontology*, **53**, 1077–1098. doi:10.1111/j.1475-4983.2010.00995.x

Bianucci, G., **Gatt, M.**, **Catanzariti, R.**, **Sorbi, S.**, **Bonavia, C. G.**, **Curmi, R.** & **Varola, A.** 2011. Systematics, biostratigraphy and evolutionary pattern of the Oligo–Miocene marine mammals from the Maltese Islands. *Geobios*, **44**, 549–585. doi:10.1016/j.geobios.2011.02.009

Bianucci, G., **Di Celma, C.**, **Urbina, M.** & **Lambert, O.** 2016. New beaked whales from the late Miocene of Peru and evidence for convergent evolution in stem and crown Ziphiidae (Cetacea, Odontoceti). *PeerJ*, **4**, e2479. doi:10.7717/peerj.2479

Bianucci, G., **Bosio, G.**, **Malinverno, E.**, **Muizon, C. de**, **Villa, I. M.**, **Urbina, M.** & **Lambert, O.** 2018a. A new large squalodelphinid (Cetacea, Odontoceti) from Peru sheds light on the Early Miocene platanistoid disparity and ecology. *Royal Society Open Science*, **5**, 172302. 10.1098/rsos.172302

Bianucci, G., **Collareta, A.**, **Bosio, G.**, **Landini, W.**, **Gariboldi, K.**, **Gioncada, A.**, **Lambert, O.**, **Malinverno, E.**, **Muizon, C. de**, **Varas-Malca R.**, **Villa, I. M.**, **Coletti, G.**, **Urbina, M.** & **Di Celma, C.** 2018b. Taphonomy and palaeoecology of the lower Miocene marine vertebrate assemblage of Ullujaya (Chilcatay Formation, East Pisco Basin, southern Peru). *Palaeogeography, Palaeoclimatology, Palaeoecology*, **511**, 256–279. doi:10.1016/j.palaeo.2018.08.013

Bloodworth, B. & **Marshall, C. D.** 2005. Feeding kinematics of *Kogia* and *Tursiops* (Odontoceti: Cetacea): characterization of suction and ram feeding. *Journal of Experimental Biology*, **208**, 3721–3730. doi:10.1242/jeb.01807

Boersma, A. T. & **Pyenson, N. D.** 2015. *Albicetus oxymycterus*, a new generic name and redescription of a basal physeteroid (Mammalia, Cetacea) from the Miocene of California, and the evolution of body size in sperm whales. *PLoS ONE*, **10**, e0135551. 10.1371/journal.pone.0135551

Boessenecker, R. W., **Fraser, D.**, **Churchill, M.** & **Geisler, J. H.** 2017. A toothless dwarf dolphin (Odontoceti:

Xenorophidae) points to explosive feeding diversification of modern whales (Neoceti). *Proceedings of the Royal Society B*, **284**, 20170531. doi:10.1098/rspb.2017.0531

Boschma, H. 1938. On the teeth and some other particulars of the sperm whale (*Physeter macrocephalus* L.). *Temminckia*, **3**, 151–278.

Bosio, G., Malinverno, E., Villa, I. M., Di Celma, C., Gariboldi, K., Gioncada, A., Barberini, V., Urbina, M. & Bianucci, G. 2020a. Tephrochronology and chronostratigraphy of the Miocene Chilcatay and Pisco formations (East Pisco Basin, Peru). *Newsletters on Stratigraphy*, **53**, 213–247. doi:10.1127/nos/2019/0525

Bosio, G., Malinverno, E., Collareta, A., Di Celma, C., Gioncada, A., Parente, M., Berra, F., Marx, F. G., Vertino, A. & Urbina, M. 2020b. Strontium isotope stratigraphy and the thermophilic fossil fauna from the middle Miocene of the East Pisco Basin (Peru). *Journal of South American Earth Sciences*, **97**, 102399. doi:10.1016/j.jsames.2019.102399

Brisson, M.-J. 1762. *Regnum Animale in classes IX distributum, sine synopsis methodica*. Theodorum Haak, Paris, 296 pp.

Buchholtz, E. A. 2001. Vertebral osteology and swimming style in living and fossil whales (Order Cetacea). *Journal of Zoology*, **253**, 175–190. doi:10.1017/S0952836901000164

Caldwell, D. K. & Caldwell, M. C. 1989. Pygmy sperm whale *Kogia breviceps* (de Blainville, 1838): dwarf sperm whale *Kogia simus* Owen, 1866. Pp. 235–260 in S. H. Ridgway & R. Harrison (eds) *Handbook of marine mammals, Volume 4: river dolphins and the larger toothed whales*. Academic Press, London.

Clarke, R. & Paliza, O. 1972. Sperm whales of the Southeast Pacific. Part III, morphometry. *Hvalrdets Skrifter*, **53**, 1–106.

Collareta, A., Fulgosi, F. C. & Bianucci, G. 2019. A new kogiid sperm whale from northern Italy supports psychrospheric conditions in the early Pliocene Mediterranean Sea. *Acta Palaeontologica Polonica*, **64**, 609–626. doi:10.4202/app.00578.2018

Collareta, A., Lambert, O., Muizon, C. de, Benites Palomino, A. M., Urbina, M. & Bianucci, G. (In press). A new physeteroid from the late Miocene of Peru expands the diversity of extinct dwarf and pygmy sperm whales (Cetacea: Odontoceti: Kogiidae). *Comptes Rendus Palevol*. doi:10.1016/j.crpv.2008.06.002

Cranford, T. W. 1999. The sperm whale's nose: sexual selection on a grand scale? *Marine Mammal Science*, **15**, 1133–1157. doi:10.1111/j.1748-7692.1999.tb00882.x

Di Celma, C., Malinverno, E., Collareta, A., Bosio, G., Gariboldi, K., Lambert, O., Landini, W., Pierantoni, P. P., Gioncada, A., Villa, I. M., Coletti, G., Muizon, C. de, Urbina, M. & Bianucci, G. 2018. Facies analysis, stratigraphy and marine vertebrate assemblage of the lower Miocene Chilcatay Formation at Ullujaya (Pisco Basin, Peru). *Journal of Maps*, **14**, 257–268. doi:10.1080/17445647.2018.1456490

Di Celma, C., Pierantoni, P. P., Malinverno, E., Collareta, A., Lambert, O., Landini, W., Bosio, G., Gariboldi, K., Gioncada, A., Muizon, C. de, Molli, G., Marx, F. G., Varas-Malca, R. M., Urbina, M. & Bianucci, G. 2019. Allostratigraphy and paleontology of the lower Miocene Chilcatay Formation in the Zamaca area, East Pisco basin, southern Peru. *Journal of Maps*, **15**, 393–405. doi:10.1080/17445647.2019.1604439

Fitzgerald, E. M. G. 2010. The morphology and systematics of *Mammalodon colliveri* (Cetacea: Mysticeti), a toothed mysticete from the Oligocene of Australia. *Zoological Journal of the Linnean Society*, **158**, 367–476. doi:10.1111/j.1096-3642.2009.00572.x

Flower, W. H. 1867a. On the osteology of the cachalot or sperm-whale (*Physeter macrocephalus*). *Transactions of the Zoological Society of London*, **6**, 309–372. doi:10.1111/j.1096-3642.1868.tb00580.x

Flower, W. H. 1867b. Description of the skeleton of *Inia geoffrensis* and the skull of *Pontoporia blainvillii*, with remarks on the systematic position of these animals in the Order Cetacea. *Transactions of the Zoological Society of London*, **6**, 87–116. doi:10.1111/j.1096-3642.1867.tb00572.x

Fordyce, R. E. & Muizon, C. de. 2001. Evolutionary history of cetaceans: a review. Pp. 169–233 in J.-M. Mazin & V. de Buffrénil (eds) *Secondary adaptation of tetrapods to life in water*. Verlag Dr. Friedrich Pfeil, München.

Fordyce, R. E., Quilty, P. G. & Daniels, J. 2002. *Australodelphis mirus*, a bizarre new toothless ziphiid-like fossil dolphin (Cetacea: Delphinidae) from the Pliocene of Vestfold Hills, East Antarctica. *Antarctic Science*, **14**, 37–54. doi:10.1017/S0954102002000561

Fraser, F. C. & Purves, P. E. 1960. Hearing in cetaceans: evolution of the accessory air sacs and the structure of the outer and middle ear in recent cetaceans. *Bulletin of the British Museum (Natural History), Zoology*, **7**, 1–140.

Galatius, A. & Kinze, C. C. 2003. Ankylosis patterns in the postcranial skeleton and hyoid bones of the harbour porpoise (*Phocoena phocoena*) in the Baltic and North Sea. *Canadian Journal of Zoology*, **81**, 1851–1861. doi:10.1139/z03-181

Gondar, D. 1975. La presencia de cetaceos Physeteridae en el Terciario Suprior ('Rionegrense') de la Provincia de Rio Negro. *Actas del Primier Congreso Argentino de Paleontologia y Biostratigrafia Tucuman, Argentina*, **2**, 349–354.

Gray, J. E. 1821. On the natural arrangement of vertebrose animals. *London Medical Repository*, **15**, 296–310.

Habegger, M. L., Dean, M. N., Dunlop, J. W., Mullins, G., Stokes, M., Huber, D. R., Winters, D. & Motta, P. J. 2015. Feeding in billfishes: inferring the role of the rostrum from a biomechanical standpoint. *Journal of Experimental Biology*, **218**, 824–836. doi:10.1242/jeb.106146

Hampe, O. 2006. Middle/late Miocene hoplocetine sperm whale remains (Odontoceti: Physeteridae) of North Germany with an emended classification of the Hoplocetinae. *Fossil Record*, **9**, 61–86. doi:10.1002/mmng.200600002

Hocking, D. P., Marx, F. G., Park, T., Fitzgerald, E. M. G. & Evans, A. R. 2017. A behavioural framework for the evolution of feeding in predatory aquatic mammals. *Proceedings of the Royal Society B*, **284**, 20162750. doi:10.1098/rspb.2016.2750

Huggenberger, S., André, M. & Oelschläger, H. H. 2016. The nose of the sperm whale: overviews of functional design, structural homologies and evolution. *Journal of the Marine Biological Association of the United Kingdom*, **96**, 783–806. doi:10.1017/S0025315414001118

Kasuya, T. 1973. Systematic consideration of recent toothed whales based on the morphology of tympano-periotic bone. *Scientific Reports of the Whales Research Institute*, **25**, 1–103.

Kellogg, R. 1925. On the occurrence of remains of fossil porpoises of the genus *Eurhinodelphis* in North America. *Proceedings of the United States National Museum*, **66**, 1–40. doi:10.5479/si.00963801.66-2563.1

Kellogg, R. 1927. Study of the skull of a fossil sperm-whale from the Temblor Miocene of southern California. *Publications of the Carnegie Institution of Washington*, **346**, 1–23. doi:10.5479/si.00963801.61-2435.1

Kellogg, R. 1936. A review of the Archaeoceti. *Carnegie Institute of Washington Publication*, **482**, 1–366.

Kellogg, R. 1965. Fossil marine mammals from the Miocene Calvert Formation of Maryland and Virginia. The Miocene Calvert sperm whale *Orycterocetus*. *Bulletin of the United States National Museum*, **247**, 47–63.

Kimura, T., Hasegawa, Y. & **Barnes, L. G.** 2006. Fossil sperm whales (Cetacea, Physeteridae) from Gunma and Ibaraki prefectures, Japan; with observations on the Miocene fossil sperm whale *Scaldicetus shigensis* Hirota and Barnes, 1995. *Bulletin of the Gunma Museum of Natural History*, **10**, 1–23.

Kurihara, N., **Amano, M.** & **Yamada, T.** 2016. Decrease in tooth count in melon-headed whales. *Journal of Zoology*, **300**, 8–17. doi:10.1111/jzo.12363

Lambert, O. 2005a. Systematics and phylogeny of the fossil beaked whales *Ziphirostrum* du Bus, 1868 and *Choneziphius* Duvernoy, 1851 (Cetacea, Odontoceti), from the Neogene of Antwerp (north of Belgium). *Geodiversitas*, **27**, 443–497.

Lambert, O. 2005b. Phylogenetic affinities of the long-snouted dolphin *Eurhinodelphis* (Cetacea, Odontoceti) from the Miocene of Antwerp. *Palaeontology*, **48**, 653–679. doi:10.1111/j.1475-4983.2005.00472.x

Lambert, O. 2005c. Review of the Miocene long-snouted dolphin *Priscodelphinus cristatus* du Bus, 1872 (Cetacea, Odontoceti) and phylogeny among eurhinodelphinids. *Bulletin de l'Institut Royal des Sciences Naturelles de Belgique, Sciences de la Terre*, **75**, 211–235.

Lambert, O. 2008. Sperm whales from the Miocene of the North Sea: a re-appraisal. *Bulletin de l'Institut Royal des Sciences Naturelles de Belgique, Sciences de la Terre*, **78**, 277–316.

Lambert, O., **Bianucci, G.**, **Post, K.**, **Muizon, C. de**, **Salas-Gismondi, R.**, **Urbina, M.** & **Reumer, J.** 2010. The giant bite of a new raptorial sperm whale from the Miocene epoch of Peru. *Nature*, **466**, 105–108. doi:10.1038/nature09067

Lambert, O., **Bianucci, G.** & **Beatty, B. L.** 2014. Bony outgrowths on the jaws of an extinct sperm whale support macroraptorial feeding in several stem physeteroids. *Naturwissenschaften*, **101**, 517–521. doi:10.1007/s00114-014-1182-2

Lambert, O., **Collareta, A.**, **Landini, W.**, **Post, K.**, **Ramassamy, B.**, **Di Celma, C.**, **Urbina, M.** & **Bianucci, G.** 2015. No deep diving: evidence of predation on epipelagic fish for a stem beaked whale from the Late Miocene of Peru. *Proceedings of the Royal Society B*, **282**, 20151530. doi:10.1098/rspb.2015.1530

Lambert, O., **Bianucci, G.** & **Muizon, C. de.** 2017. Macroraptorial sperm whales (Cetacea, Odontoceti, Physeteroidea) from the Miocene of Peru. *Zoological Journal of the Linnean Society*, **179**, 404–474. doi:10.1111/zoj.12456

Lambert, O., **Muizon, C. de**, **Malinverno, E.**, **Di Celma, C.**, **Urbina, M.** & **Bianucci, G.** 2018. A new odontocete (toothed cetacean) from the early Miocene of Peru expands the morphological disparity of extinct heterodont dolphins. *Journal of Systematic Palaeontology*, **16**, 981–1016. doi:10.1080/14772019.2017.1359689

Lambert, O. & **Bianucci, G.** 2019. How to break a sperm whale's teeth: dental damage in a large Miocene physeteroid from the North Sea basin. *Journal of Vertebrate Paleontology*, **39**, e1660987. doi:10.1080/02724634.2019.1660987

Landini, W., **Collareta, A.**, **Di Celma, C.**, **Malinverno, E.**, **Urbina, M.** & **Bianucci, G.** 2019. The early Miocene elasmobranch assemblage from Zamaca (Chilcatay Formation, Peru). *Journal of South American Earth Sciences*, **91**, 352–371. doi:10.1016/j.jsames.2018.08.004

Lydekker, R. 1893. Contribution to the knowledge of the fossil vertebrates of Argentina. Part II. Cetacean skulls from Patagonia. *Anales del Museo de La Plata*, **1893**, 1–14.

Marx, F. G., **Lambert, O.** & **Uhen, M. D.** 2016. *Cetacean paleobiology*. John Wiley & Sons, Chichester (UK), 319 pp.

McCurry, M. R. & **Pyenson, N. D.** 2018. Hyper-longirostry and kinematic disparity in extinct toothed whales. *Paleobiology*, **45**, 21–29. doi:10.1017/pab.2018.33

Mchedlidze, G. A. 1976. *General features of the palaeobiological evolution of Cetacea*. [Osnovnye Cherty Paleobiologicheskoi Istorii Kitoobraznykh]. Metsniereba Publishers, translated from Russian in 1984 by Amerind Publishing Co. Pvt. Ltd., New Delhi, 139 pp.

Mead, J. G. & **Payne, R. S.** 1975. A specimen of the Tasman beaked whale, *Tasmacetus shepherdi*, from Argentina. *Journal of Mammalogy*, **56**, 213–218. doi:10.2307/1379619

Mead, J. G. & **Fordyce, R. E.** 2009. The therian skull: a lexicon with emphasis on the odontocetes. Smithsonian *Contributions to Zoology*, **627**, 1–248. doi:10.5479/si.00810282.627

Moore, J. C. 1968. Relationships among the living genera of beaked whales. *Fieldiana: Zoology*, **53**, 209–298.

Moran, M. M., **Bajpai, S.**, **George, J. C.**, **Suydam, R.**, **Usip, S.** & **Thewissen J. M. G.** 2015. Intervertebral and epiphyseal fusion in the postnatal ontogeny of cetaceans and terrestrial mammals. *Journal of Mammalian Evolution*, **22**, 93–109. doi:10.1007/s10914-014-9256-7

Muizon, C., de. 1984. Les vertébrés de la Formation Pisco (Pérou). Deuxième partie: les Odontocètes (Cetacea, Mammalia) du Pliocène inférieur de Sud-Sacaco. *Travaux de l'Institut Français d'Etudes Andines*, **27**, 1–188.

Muizon, C., de. 1988. Les vertébrés fossiles de la Formation Pisco (Pérou). Troisième partie: les Odontocètes (Cetacea, Mammalia) du Miocène. *Travaux de l'Institut Français d'Etudes Andines*, **42**, 1–244.

Muizon, C., de. 1991. A new Ziphiidae (Cetacea) from the Early Miocene of Washington State (USA) and phylogenetic analysis of the major groups of odontocetes. *Bulletin du Muséum National d'Histoire Naturelle, Paris*, **12**, 279–326.

Omura, H., **Nishiwaki, M.**, **Ichihara, T.** & **Kasuya, T.** 1962. Osteological note of a sperm whale. *Scientific Reports of the Whales Research Institute*, **16**, 35–45.

Paolucci, F., **Buono, M. R.**, **Fernández, M. S.**, **Marx, F. G.** & **Cuitiño, J. I.** 2020. *Diaphorocetus poucheti* (Cetacea, Odontoceti, Physeteroidea) from Patagonia, Argentina: one of the earliest sperm whales. *Journal of Systematic Palaeontology*, **18**, 335–355. doi:10.1080/14772019.2019.1605544

Pierce, K. V. & **Kajimura, H.** 1980. Acid etching and highlighting for defining growth layers in cetacean teeth. *Reports of the International Whaling Commission Special Issue*, **3**, 99–103.

Pyenson, N. D. & **Sponberg, S. N.** 2011. Reconstructing body size in extinct crown Cetacea (Neoceti) using allometry, phylogenetic methods and tests from the fossil record. *Journal of Mammalian Evolution*, **18**, 269–288. doi:10.1007/s10914-011-9170-1

Racicot, R. A., **Deméré, T. A.**, **Beatty, B. L.** & **Boessenecker, R. W.** 2014. Unique feeding morphology in a new prognathous extinct porpoise from the Pliocene of California. *Current Biology*, **24**, 774–779. doi:10.1016/j.cub.2014.02.031

Rice, D. W. 1989. Sperm whale *Physeter macrocephalus* Linnaeus, 1758. Pp. 177–233 in S. H. Ridgway & R. Harrison (eds) *Handbook of marine mammals, Volume 4: river dolphins and the larger toothed whales*. Academic Press, London.

Ross, G. J. B. 1984. The smaller cetaceans of the south east coast of southern Africa. *Annals of the Cape Provincial Museums of Natural History*, **15**, 173–410.

Schulte, H. von W. & **Smith, M. de F.** 1918. The external characters, skeletal muscles, and peripheral nerves of *Kogia breviceps* (Blainville). *Bulletin of the American Museum of Natural History*, **38**, 7–72.

Staudinger, M. D., **McAlarney, R. J.**, **McLellan, W. A.** & **Pabst, A. D.** 2014. Foraging ecology and niche overlap in pygmy (*Kogia breviceps*) and dwarf (*Kogia sima*) sperm whales from waters of the US mid-Atlantic coast. *Marine Mammal Science*, **30**, 626–655. doi:10.1111/mms.12064

Swofford, D. L. 2001. *PAUP*. Phylogenetic analysis using parsimony (*and other methods). Version 4b10*. Sinauer Associates, Sunderland, Massachusetts.

Tanaka, Y. & **Fordyce, R. E.** 2017. *Awamokoa tokarahi*, a new basal dolphin in the Platanistoidea (late Oligocene, New Zealand). *Journal of Systematic Palaeontology*, **15**, 365–386. doi:10.1080/14772019.2016.1202339

Thornton, S. W., **McLellan, W. A.**, **Rommel, S. A.**, **Dillaman, R. M.**, **Nowacek, D. P.**, **Koopman, H. N.** & **Pabst, A. D.** 2015. Morphology of the nasal apparatus in pygmy (*Kogia breviceps*) and dwarf (*K. sima*) sperm whales. *The Anatomical Record*, **298**, 1301–1326. doi:10.1002/ar.23168

True, F. W. 1910. An account of the beaked whales of the family Ziphiidae in the collection of the United States National Museum, with remarks on some specimens in other American museums. *Bulletin of the United States National Museum*, **73**, 1–89.

Uhen, M. D. 2008. New protocetid whales from Alabama and Mississippi, and a new cetacean clade, Pelagiceti. *Journal of Vertebrate Paleontology*, **28**, 589–593.

Van Beneden, P.-J. & **Gervais, P.** 1880. *Ostéographie des cétacés vivants et fossiles*. Arthus Bertrand, Paris, 634 pp.

Velez-Juarbe, J., **Wood, A. R.**, **De Gracia, C.** & **Hendy, A. J. W.** 2015. Evolutionary patterns among living and fossil kogiid sperm whales: evidence from the Neogene of Central America. *PLoS ONE*, **10**, e0123909. doi:10.1371/journal.pone.0123909

Vélez-Juarbe, J., **Wood, A. R.** & **Pimiento, C.** 2016. Pygmy sperm whales (Odontoceti, Kogiidae) from the Pliocene of Florida and North Carolina. *Journal of Vertebrate Paleontology*, **36**, e1135806. doi:10.1080/02724634.2016.1135806

Watwood, S. L., **Miller, P. J. O.**, **Johnson, M.**, **Madsen, P. T.** & **Tyack, P. L.** 2006. Deep-diving foraging behaviour of sperm whales (*Physeter macrocephalus*). *Journal of Animal Ecology*, **75**, 814–825. doi:10.1111/j.1365-2656.2006.01101.x

Werth, A. J. 2004. Functional morphology of the sperm whale tongue, with reference to suction feeding. *Aquatic Mammals*, **30**, 405–418. doi:10.1578/AM.30.3.2004.405

Werth, A. J. 2006. Mandibular and dental variation and the evolution of suction feeding in Odontoceti. *Journal of Mammalogy*, **87**, 579–588. doi:10.1644/05-MAMM-A-279R1.1

Yamada, M. 1954. Some remarks on the pygmy sperm whale, *Kogia*. *Scientific Reports of the Whales Research Institute*, **9**, 37–61.

Associate Editor: Adrian Lister